Evaluation of Drilling Mud Dispersion Models at SOEI Tier I Sites: Part 1 North Triumph, Fall 1999.

C.G. Hannah, A. Drozdowski, D.K. Muschenheim,
J.W. Loder, S. Belford, M. MacNeil

Ocean Sciences Division
Maritimes Region
Fisheries and Oceans Canada

Bedford Institute of Oceanography
P.O. Box 1006
Dartmouth, Nova Scotia
Canada B2Y 4A2

2003

Canadian Technical Report of Hydrography and Ocean Sciences 232

Fisheries and Oceans Canada | Pêches et Océans Canada

Canada

Canadian Technical Report of
Hydrography and Ocean Sciences 232

2003

Evaluation of Drilling Mud Dispersion Models at SOEI Tier I Sites: Part 1 North Triumph, Fall 1999.

by

C. G. Hannah, A. Drozdowski, D. K. Muschenheim[1],
J. W. Loder, S. Belford[2], M. MacNeil[3]

Ocean Sciences Division
Maritimes Region
Fisheries and Oceans Canada

Bedford Institute of Oceanography
P.O. Box 1006
Dartmouth, N.S.
Canada B2Y 4A2

[1]Acadia Centre for Estuarine Research, Acadia University, Wolfville, NS
[2]Jacques Whitford Environment Limited, Dartmouth, NS
[3]Coastal Ocean Associates, Dartmouth, NS

©Her Majesty the Queen in Right of Canada 2003
Cat. No. Fs 97-18/232E ISSN 0711-6764

Correct citation for this publication:

Hannah, C.G., A. Drozdowski, D. K. Muschenheim, J.W. Loder, S. Belford, and M. MacNeil, 2003. Evaluation of Drilling Mud Dispersion Models at SOEI Tier I Sites: Part 1 North Triumph, Fall 1999. Can. Tech. Rep. Hydrogr. Ocean Sci. 232: v+51 pp.

104-00166/

Contents

List of Figures iv

List of Tables iv

Abstract/Résumé v

1 Introduction 1

2 Methods 2
- 2.1 The `bblt` Model . . . 3
- 2.2 Currents . . . 5
- 2.3 Waves . . . 8
- 2.4 Bottom Stress . . . 8
- 2.5 Settling Velocity . . . 8
- 2.6 Boundary Layer Height . . . 10
- 2.7 Drilling Discharge . . . 10
- 2.8 EEM Program Sampling . . . 13
- 2.9 `bblt` Simulations . . . 17

3 Results 18
- 3.1 Bottom Stress and Median Height . . . 18
- 3.2 The EEM Data . . . 19
- 3.3 Comparison With EEM Data . . . 21
- 3.4 Near-bottom Concentration . . . 27

4 Discussion 33

5 Conclusions 37

References 39

A Details of Gap Filling and Vertical Extrapolation of the ADCP Data 42

B Details of Extrapolation in Time of the ADCP Data 48

C Vertical Profiles at North Triumph 50

List of Figures

1 The North Triumph site on Sable Island Bank 3
2 Schematic of inputs, outputs and processes. 4
3 Time lines of observations at North Triumph 5
4 Waves, bottom currents, and friction velocity 6
5 The stress-dependent settling velocity 9
6 Density profiles used to estimate h_{max} 11
7 The hourly discharge time series 12
8 The location map of the suspended barite observations 15
9 Time until next breakup event 19
10 Median Sediment Height 20
11 Suspended barium as a function of distance from the rig 20
12 The timing of the simulation events. 22
13 Concentration at 0.5 mab for selected observation locations 23
14 Predicted concentration distribution at 0.5 mab for each location 24
15 The frequency of occurrence for different concentration levels at 0.5 mab 25
16 Concentration as a function of distance from rig 26
17 Near-bottom concentration time series at observation locations 28
18 Time spent above 1.0, 10 and 100 $\mu g\,L^{-1}$ during 28 Oct. to 5 Nov. 1999 . 29
19 Total time above 100, 1000 and 10000 $\mu g\,L^{-1}$ for variable settling (high) . 30
20 Total time above 100, 1000 and 10000 $\mu g\,L^{-1}$ for variable settling (low) . 30
21 Total time above 100, 1000 and 10000 $\mu g\,L^{-1}$ for constant settling (high) 31
22 Total time above 100, 1000 and 10000 $\mu g\,L^{-1}$ for constant settling (low) . 31
23 Variability in exposure time 32
24 Friction Velocity and 3 mab currents for NT and Hib. 35
25 TS2 residual current with filled gaps 45
26 TS3 currents below 8 mab versus the 8 mab current 47
27 Extrapolated bottom current and stress 49
28 Vertical profiles of mean velocity 51

List of Tables

1 Dates and locations for the 1999 ADCP deployments 5
2 ADCP vertical information 7
3 Observations of suspended barium and barite 16
4 Parameter values used for `bblt` runs 17
5 Classification of gaps in TS2 43
6 Least square fit parameters and rms errors 46

Abstract

Hannah, C.G., A. Drozdowski, D. K. Muschenheim, J.W. Loder, S. Belford, and M. MacNeil, 2003. Evaluation of Drilling Mud Dispersion Models at SOEI Tier I Sites: Part 1 North Triumph, Fall 1999. Can. Tech. Rep. Hydrogr. Ocean Sci. 232: v+51 pp.

The `bblt` model (benthic boundary layer transport model) was used to simulate the drift and dispersion of suspended drilling muds near North Triumph on Sable Island Bank during a drilling program in the fall of 1999. The simulations focussed on barite ($BaSO_4$), the primary weighting agent used in the drill muds. The goal was to use the observations of barium in the water column obtained by the Environmental Effects Monitoring (EEM) program to test the model. The model was able to reproduce the very low concentrations (generally $< 1\ \mu g\,L^{-1}$) observed during the EEM program. Over the entire drilling program, the model also predicts barite concentrations $> 100\ \mu g\,L^{-1}$ ($= 0.1\ mg\,L^{-1}$, the no effects concentration for scallops) for several days within a few kilometres of the rig. However there were no EEM observations during periods of active discharge to validate this prediction.

Résumé

Hannah, C.G., A. Drozdowski, D. K. Muschenheim, J.W. Loder, S. Belford, and M. MacNeil, 2003. Evaluation of Drilling Mud Dispersion Models at SOEI Tier I Sites: Part 1 North Triumph, Fall 1999. Can. Tech. Rep. Hydrogr. Ocean Sci. 232: v+51 pp.

On a utilisé le modèle bblt, benthic boundary layer transport (modèle de transport de la couche limite benthique) pour simuler la dérive et la dispersion des boues de forage en suspension près du site North Triumph sur le banc de l'Île de Sable au cours d'un programme de forage qui s'est déroulé à l'automne 1999. Les simulations ont porté sur la barytine ($BaSO_4$), principal alourdissant utilisé dans les boues de forage. L'objectif était d'utiliser les observations sur le baryum dans la colonne d'eau obtenues grâce au programme de suivi des effets sur l'environnement (SEE) pour faire l'essai du modèle. Le modèle permettait de reproduire les très faibles concentrations (généralement $< 1\ \mu g\,L^{-1}$) observées au cours du programme SEE. Pendant toute la durée du programme de forages, le modèle a prévu des concentrations de barytine supérieures à $100\ \mu g\,L^{-1}$ ($= 0.1\ mg\,L^{-1}$, la valeur seuil de non-effet sur la concentration des pétoncles) pendant plusieurs jours, dans un rayon de quelques kilomètres de l'installation de forage. Toutefois, il n'y a pas eu d'observations dans le cadre du SEE au cours des périodes de décharge active pour valider cette prévision.

1 Introduction

The fate and potential environmental impacts of discharged drilling muds are ongoing issues to offshore petroleum operators, regulators, government agencies and environmentalists, particularly with multiple development and exploration sites in close proximity of each other on Sable Bank and the northeast Grand Bank (e.g. Gordon et al. 2000). Sound scientific assessments of the fate and impacts for different mud/discharge scenarios can provide a basis for prudent decisions and cost-effective strategies that minimize both real and perceived adverse impacts. Validated or calibrated dispersion models can be an effective tool in environmental impacts assessments and in waste management planning.

Through funding from the federal Panel for Energy Research and Development (PERD) and cooperation with industry, DFO scientists and contractors have developed a series of mud dispersion models (referred to as "benthic boundary layer transport" or `bblt` models) that include important shear dispersion processes not represented in previous models. The focus here is on the local form of the `bblt` model (henceforth `bblt`) (Hannah et al. 1995; Tedford et al. 2001) which assumes no horizontal variation in the physical environment. Earlier versions of `bblt` have been used in evaluations (MacLaren Plansearch Ltd. 1997) for the Environmental Impacts Assessment Report for the Sable Offshore Energy Project (SOEP), in a DFO assessment of potential effects of exploration drilling on Georges Bank (Gordon et al. 2000), in the generic "Environmental Assessment of Exploration Drilling off Nova Scotia" (Thomson et al., 2000) carried out for CNSOPB and industry, and in evaluations of mud drift and dispersion at the Hibernia production site on the Grand Bank (Tedford et al., 2003). However, a limiting factor in realizing the potential and confidence of `bblt` for impacts assessment and waste management planning has been the lack of concurrent observational datasets on discharges, the physical environment and mud distributions for validating the model and its parameterizations.

This report describes initial results from a project entitled "Field Verification of Benthic Boundary Layer Modelling Effects" funded by the Environmental Sciences Research Fund (ESRF), with complementary support from DFO and PERD. The approach of the project was to evaluate the latest version of `bblt` using existing observational data from selected SOEP Tier I drill sites on Sable Bank during 1998-1999 when water-based drill muds (WBMs) were discharged into the environment. The potential datasets included: 1) the volume and properties of discharged drill muds from logsheets maintained during drilling operations; 2) time series of currents and waves at the drill sites from moored measurements during SOEP's Physical Environmental Program (e.g. COA 2000), and 3) distributions of drill muds and constituents from SOEP's Environmental Effects Monitoring (EEM) Program (SOEI, 2000).

The initial step in the project was to identify the WBM discharge periods with and followed by currents and waves time series data, and preceding or during the semi-annual EEM surveys. Such periods were found to be much less frequent than expected

due to intermittent currents and waves data, and suboptimal timing between the EEM surveys and drilling periods. Two discharge sites and periods were identified for further evaluation: a) the discharge from a single well (NT-1) at the North Triumph site in approximately 75 m water depth during September-October 1999, prior to the November 1999 EEM survey; and b) discharges from five wells during 1998 and 1999 from the shallower (water depth of 20 m) Venture site near Sable Island.

This report describes the application of `bblt` to predict the concentration of suspended drill muds near the North Triumph site south of Sable Island (Figure 1), during and following drilling in October 1999. The simulations focused on barium sulfate or barite ($BaSO_4$), the primary weighting agent in the WBMs used, and a compound shown to have an impact on sea scallops in laboratory experiments (Cranford et al., 1999). The goal was to test `bblt` using the observations of barium in the water column obtained by the SOEP EEM survey during 28 Oct. to 5 Nov. 1999.

The `bblt` simulations require time series data of discharged muds, velocity and waves. The drilling discharge time series was extracted from the drilling logs sheets. Unfortunately, the ADCP (Acoustic Doppler Current Profiler) and wave buoy at the site were both disabled by a storm during the drilling program. This meant that there were no velocity or wave observations for 9 days prior to the EEM survey and during the 7 days of the survey. The velocity data for these periods were provided by synthetic current time series constructed from the statistical properties of the ADCP observations. The missing wave time series, required for the bottom stress calculation, were taken from AES40 wave hindcast (Swail et al., 1998; Swail and Cox, 2000).

The missing velocity data meant that we could not conduct a spatially explicit comparison of the observed and simulated concentrations as we did not know the currents in a deterministic sense prior to and during the observation period. The synthetic currents time series were reconstructed with statistical methods and thus the results required a comparison more statistical in nature.

2 Methods

This section describes the observational data and model parameters used in this study. The description includes `bblt` model parameters such as settling velocity and maximum sediment height; data inputs such as drill mud discharge, currents, waves and bottom stress; and field observations of water-column barium concentration.

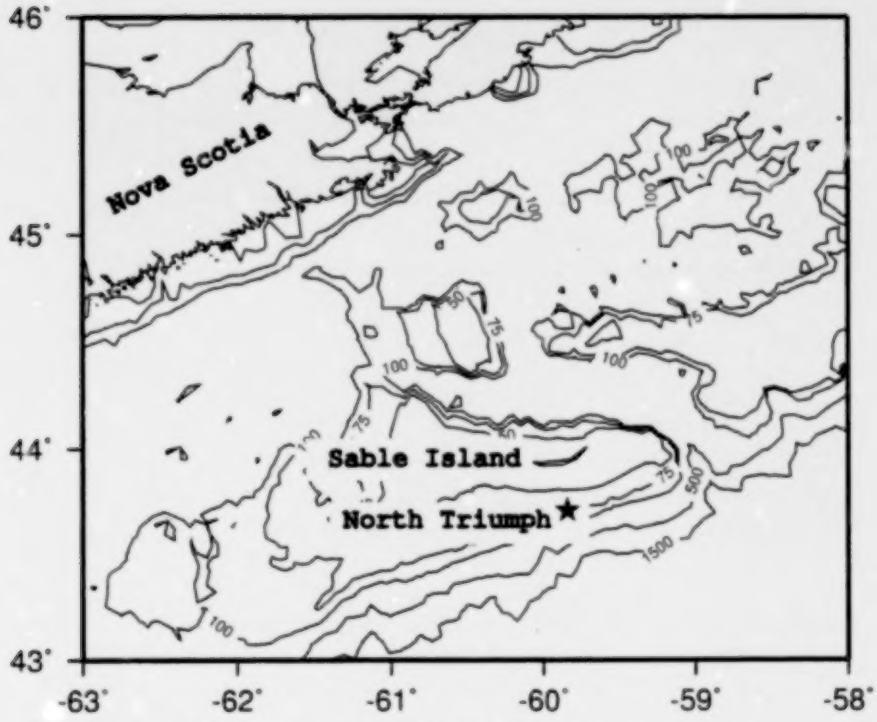

Figure 1: The North Triumph site on Sable Island Bank. Depth contours are shown in meters.

2.1 The bblt Model

bblt provides a framework for combining observations of currents and estimates of bottom stress with a description of the vertical distribution of the suspended sediment to estimate the drift, dispersion and concentration of suspended sediment (Figure 2). The vertical distribution of the suspended sediment is assumed to depend on the bottom stress and the effective settling velocity of the sediment according to the Rouse profile (Rouse, 1937):

$$c(z) = c_a(a/z)^p \tag{1}$$

where $c(z)$ is the concentration profile, $z = 0$ at the sea floor and is positive upward, c_a is the concentration at the reference height $z = a$, $p = w/(\kappa u_*)$, w is the effective settling velocity, the von Karman constant $\kappa = 0.4$, and u_* is the friction velocity. The friction velocity is given by $u_* = (\tau_b/\rho)^{1/2}$, where τ_b is the magnitude of the bottom stress and ρ is the density of water.

The core of bblt is described in Hannah et al. (1995) and Tedford et al. (2001) and the modelling procedures used herein are described in detail in Tedford et al. (2003). The two primary differences between the version of bblt used here and that used in

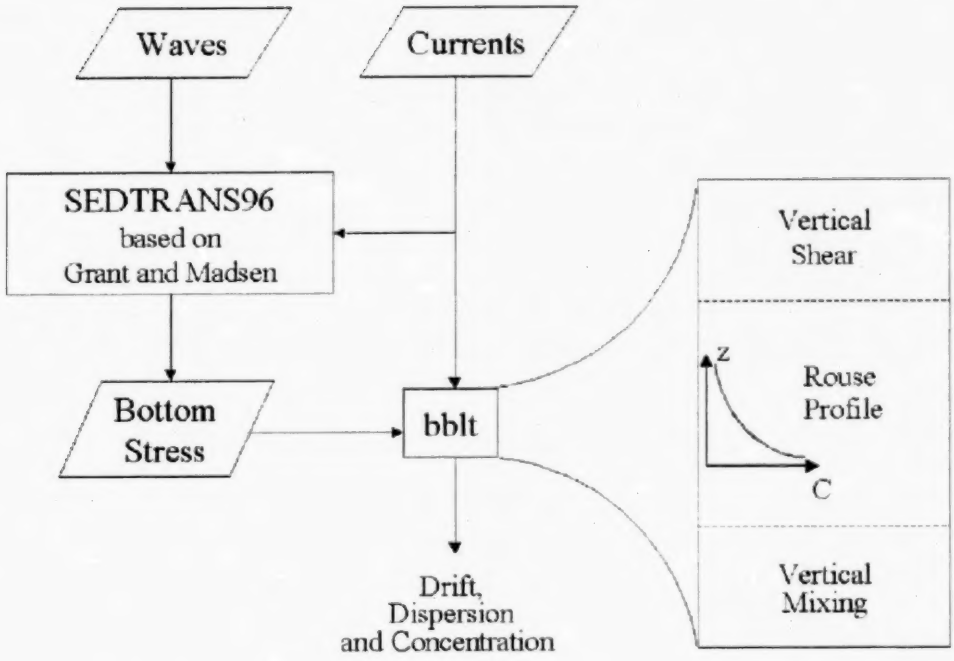

Figure 2: Schematic illustrating interaction between `bblt` and SEDTRANS96. Vertical shear, the Rouse profile and vertical mixing are the primary components of the `bblt` model.

Tedford et al. (2003) are: 1) the option for the stress-dependent settling velocity (see Section 2.5) and the ability to specify an arbitrary time series of drill mud discharge have been integrated into a single code and 2) the calculation of the sediment concentration was modified.

In the previous version of `bblt`, the volumetric concentration was calculated by counting particles in the specified volume (a cylinder defined by a central point, a radius and a top and bottom). In the simulations reported here, the concentrations during the EEM observations were very small because most of the material had left the vicinity of the rig. As a result, there were not enough particles in the vicinity of the rig for the 3-d particle counting method to provide robust estimates of the volumetric concentrations at the required horizontal and vertical scales. This is a drawback of particle based methods.

The new calculation takes advantage of the fact that the vertical distribution of the material is known. The concentration is calculated by counting all the particles in a cylinder extending from the bottom to the surface and then inferring the concentration

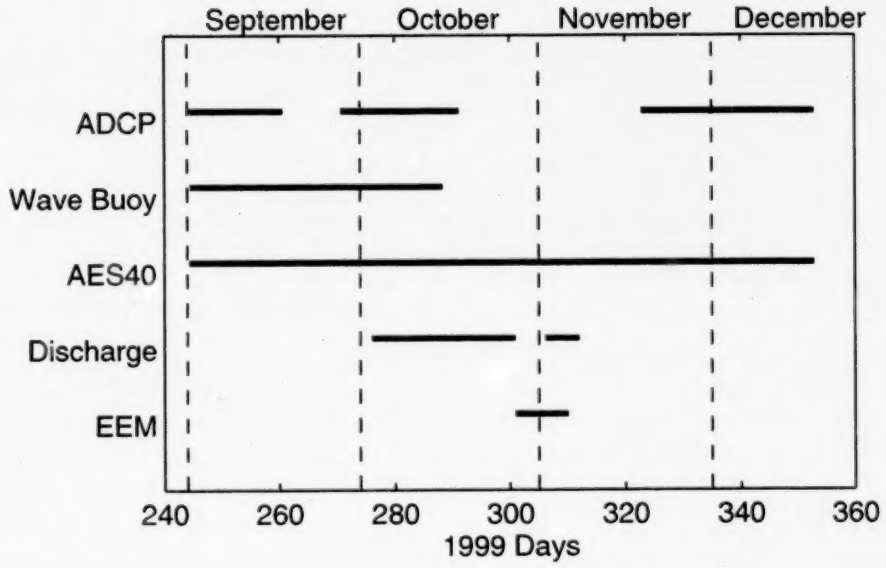

Figure 3: Time lines of current, wave, discharge and EEM observation data at North Triumph for fall of 1999.

Table 1: Date and location information for the 1999 ADCP deployment at North Triumph.

Series	Start-End	1999 Days	Length (days)	Lat	Lon
TS1	1-17 Sept.	244.4-260.6	16.2	$43^o42.7'$	$-59^o50.5'$
TS2	27 Sept. - 19 Oct.	270.7-291.3	21.6	$43^o42.7'$	$-59^o50.5'$
TS3	18 Nov. - 18 Dec.	322.9-352.9	30.0	$43^o43.2'$	$-59^o50.4'$

in a specified vertical interval using the Rouse profile (1). The stress-dependent settling velocity (Section 2.5) leads to the sediment having two components with different settling velocities and hence different Rouse profiles. The components were treated individually and then recombined into the total concentration.

2.2 Currents

Three ADCP deployments were carried out in the fall of 1999 at the North Triumph location as part of the SOEP Physical Environment Program conducted by Coastal Ocean Associates Ltd. (COA, 2000). They will be referred to as TS1, TS2, and TS3 (see Tables 1 and 2 and Figure 3 for details). The processed data files were in east-north format and had 1 m vertical resolution. The files were available in two time resolutions: 15 and 60 min. The 60 min. resolution data were considered sufficient for the modelling

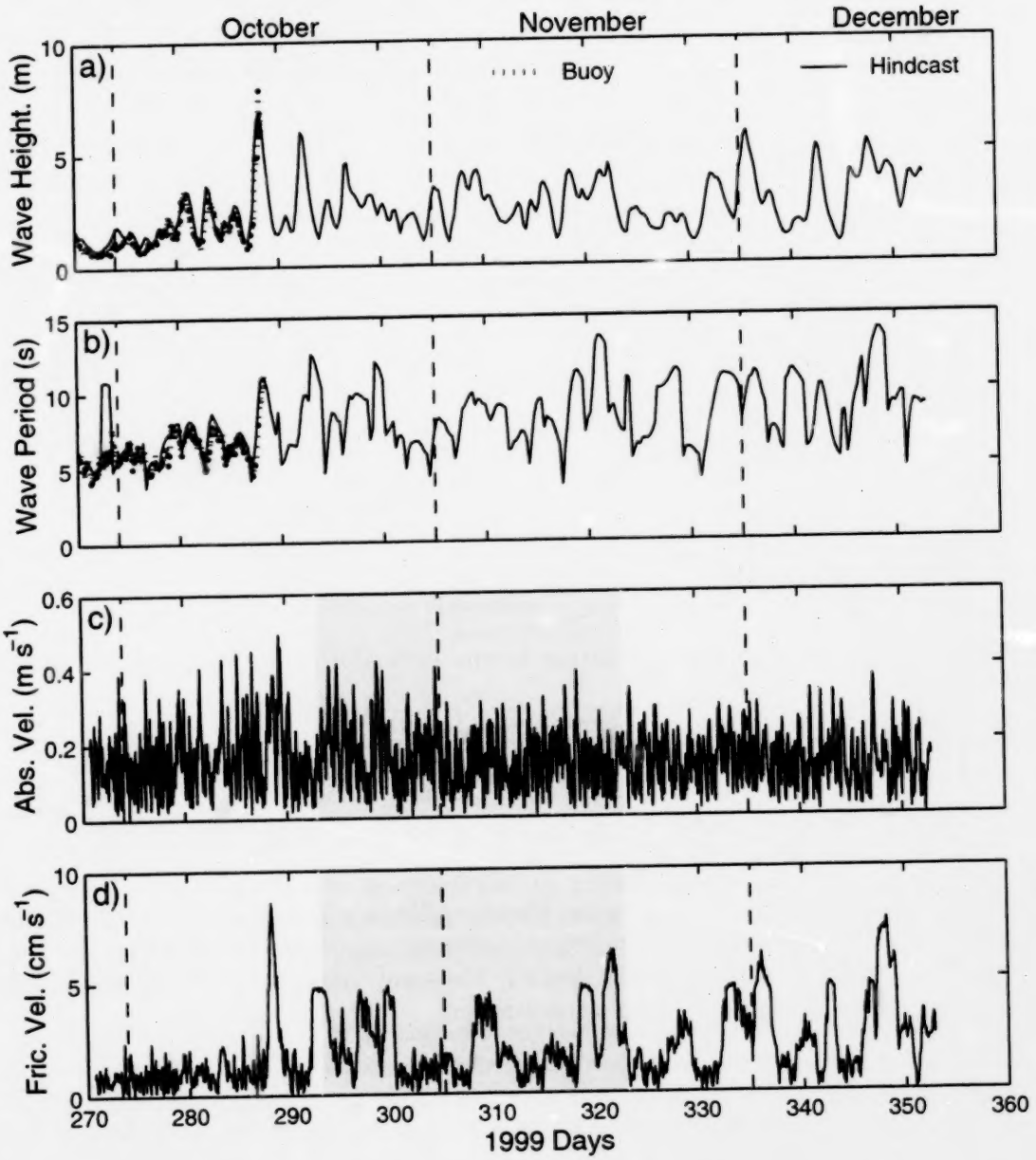

Figure 4: Shown are a) wave height (hindcast and buoy); b) wave period (hindcast and buoy); c) bottom currents speed (3 mab); d) friction velocity (u_{*cw}). There were no observed currents between the days 291.3-322.9 (shaded region on plot). The currents and bottom stress shown in this period are from one realization of the synthetic currents.

Table 2: ADCP vertical information

Series	Lowest*	Highest*	Orientation	Depth
TS1	3 m	62 m	up	70 m
TS2	8 m	66 m	down	70 m
TS3	3 m	62 m	up	69 m

* Height of bin above sea bottom (m)

here and were adopted henceforth.

The ADCP in the TS2 deployment was downward-looking. As a result the level closest to the bottom was 8 mab (metres above bottom). There were no data below this because of the common problem of sidelobe backscatter from the bottom contaminating the lowest 10% of the water column. Similarly the upward-looking ADCP measurements (TS1 and TS3) were unable to resolve the upper 10% of the water column due to sidelobe backscatter from the sea surface.

Analysis of TS3 revealed that during the deployment, the ADCP and its frame sank about 1 m in the sand (Patrick Roussel, COA, pers. comm.). This raised concerns as to the validity of the data. The data were split into the first and last 20 days for analysis purposes. Comparison of the 2 parts yielded no substantial differences in the magnitude of the currents or the near-bottom velocity profile and the TS3 data were used in the study without any corrections.

The estimated distance of the first bin of TS1 and TS3 above the sea floor was 3.25 m (Patrick Roussel, COA, pers. comm.). This was rounded to 3 mab for the modelling purposes.

TS2 had data gaps in the levels below 21 mab which were likely due to ADCP signal backscatter from suspended sand. `bblt` requires a uniform time grid for all time series. The gaps were filled using the existing sections and the 21 mab level. A further problem of TS2 was that its lowest level was at 8 mab. `bblt` interpolates from the lowest available level down to the bottom with the logarithmic sublayer (Tedford et al. 2001). In order to improve the log layer accuracy it is preferable to have 3 mab for the bottom level and hence the 8 mab level was extrapolated down to 3 mab using the statistical relationship from the corresponding levels of TS3. In this way `bblt` only extrapolates from 3 mab to the bottom. The techniques for filling the gaps (8-20 mab) and extrapolating below 8 mab (3-7 mab) are described in Appendix A.

The TS1 data were not required for the simulations because the drilling mud discharges started on 3 Oct. 1999, after the beginning of TS2. The measurements of suspended barium concentrations were made during the period 28 Oct. to 5 Nov. 1999, which falls in the gap between TS2 and TS3. Thus for modelling purposes TS2 and TS3 had to be combined into a single time series and the gap from 19 Oct. to 18 Nov. 1999 filled. The gap filling technique, described in Appendix B, was statistical in nature

and produced 10 different realizations of the currents referred to here after as synthetic currents. One realization of the near-bottom currents (3 mab) for the entire period 27 Sept.- 18 Dec. is shown in Figure 4c.

2.3 Waves

Data from a wave buoy are available for the period 1 Sept. - 16 Oct. 1999 (Coastal Ocean Associates, Dartmouth, NS). The storm on 16 Oct. rendered the buoy inoperable. Wave data from the AES40 hindcast data product (Swail et al., 1998; Swail and Cox, 2000) are available for the entire period. Figure 4a and 4b show the wave height and period for the fall of 1999 and Figure 3 shows how the wave data coincides with other measurements at the location. The excellent agreement between the buoy data and the AES40 hindcast provides confidence in the use of the hindcast for the `bblt` simulations. The hindcast data were linearly interpolated from their 6 hour time resolution to the 1 hour resolution of the currents for use in the bottom stress calculation.

2.4 Bottom Stress

The sediment transport model SEDTRANS96 (Li and Amos, 2001) was used to calculate the bottom stress and corresponding friction velocity (u_*, with units of m s^{-1}) based on the observed currents and waves. SEDTRANS96 calculates several different components of the friction velocity. We used the total stress due to currents and waves (u_{*cw}, Figure 4d) and the total stress due to the current (u_{*c}). Tedford et al. (2003) provide a discussion of the different types of friction velocity. An integral part of the SEDTRANS96 procedure, is the joint calculation of friction velocity and bed-form types, ripple height and ripple wavelength. For this application the sediment grain diameter was set to 0.25 mm based on the surfical sediment type (Anderson, 2001). At each time step, the initial ripple height and wavelength values required by SEDTRANS were set to the values from the previous time step (pers. comm. Carl Anderson).

In the present application, the waves dominate u_{*cw}. This can be seen in Figure 4 where the peaks in the friction velocity correspond to the peaks in the wave height and period. As well, Figure 27 (Appendix B) shows that the different realizations of the 3 mab currents do not have a large impact on the friction velocity.

2.5 Settling Velocity

The stress-dependent settling velocity introduced by Tedford et al. (2002) was used in this project (Figure 5). Flocs are initially assigned a fast settling velocity ($w_0 = 0.5$ cm s^{-1}) to match the large flocs expected to occur in the early stages (high concentration) of the

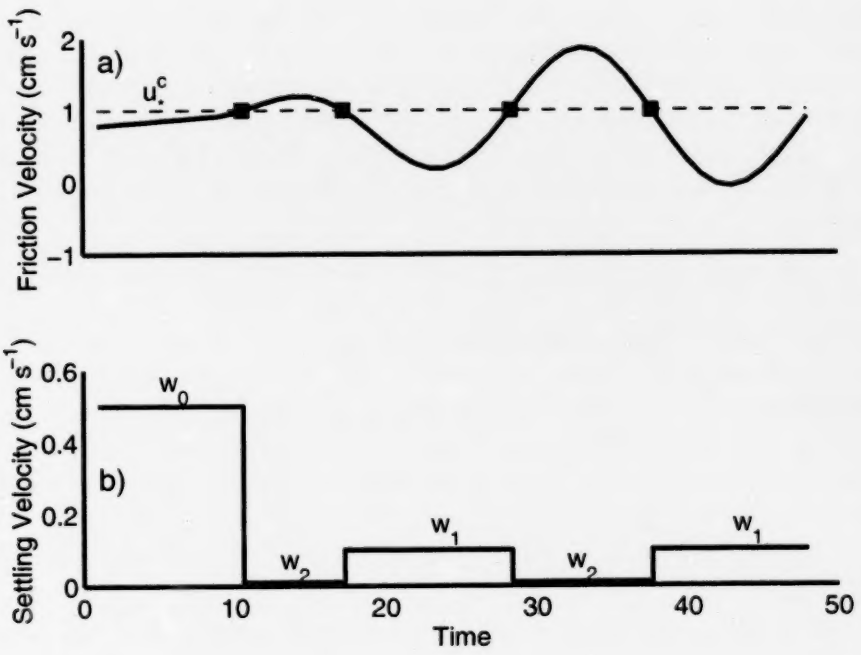

Figure 5: An illustration of the stress-dependent settling velocity: a) simplified time series of friction velocity; b) time series of the settling velocity. The square markers in a) show when breakup/flocculation occurs.

discharge plume. This settling velocity will give large near-bottom concentrations under most conditions. The settling velocity remains at this value until the friction velocity exceeds the critical value u_*^c when the flocs breakup into their individual components which have a very slow settling velocity of $w_2 = 0.01$ cm s^{-1}. This leads to a nearly uniform vertical distributions. When the friction velocity once again falls below u_*^c, the material becomes incorporated into the background of marine flocs with settling velocity $w_1 = 0.1$ cm s^{-1}. Thereafter the settling velocity is w_1 when the friction velocity is less than u_*^c and w_2 when greater. The value used for w_0 is the modal value of flocs observed by Milligan and Hill (1998) in their flocculation experiments with water based muds. The value of w_1 is based on settling velocity observations made elsewhere for naturally occurring marine flocs (Hill et al., 1998, 2000). We used $u_*^c = 1.0$ cm s^{-1} (equivalent to 0.1 Pa) for the critical stress of floc breakup (Hill et al., 2001). This approach is most applicable to the bulk discharge of water-based mud, when the large discharge volumes can create a high concentration plume where rapid flocculation can occur.

The settling velocity model proposed here assumes that the flocculation is instantaneous. While not instantaneous, Hill et al. (2001) estimate a flocculation time scale of 900 seconds, which is shorter than the hourly time scale of the currents observations.

The total friction velocity u_{*cw} is so large that the large flocs do not survive very long (Section 3.1). Also barite is a mineral grain that does not break up under high stress. As an alternative to the breakup model described above, we also considered a simple model with constant settling velocity $w_1 = 0.1$ cm s^{-1} based on the modal grain size for barite from water based mud (pers. comm. Tim Milligan, BIO). This model used u_{*c} for the friction velocity as this may be more appropriate outside the wave boundary layer (Li and Amos, 2001).

2.6 Boundary Layer Height

The Rouse profile (1) which defines the vertical distribution of sediment in `bblt` was derived for an unstratified fluid (Rouse 1937). The waters near Sable Island, however, exhibit significant stratification during the fall. Figure 6 shows density profiles from the 9 CTD casts from the fall of 1999 as well as the climatology for the area. These were obtained from the BIO archives. All 9 casts show a surface mixed layer and several show a thick bottom mixed layer.

In order to use `bblt` in stratified waters, we need to restrict the vertical extent of the concentration profile and assign it a maximum height (h_{max}). Our ability to characterize the thickness of the bottom boundary layer is limited by the small number of profiles, their broad spatial distribution (entire Sable Island Bank) and the large range in bottom depths. On the other hand, the thickness of the surface layers varies systematically from about 25 m at the end of September to 40 m in early November to 50 m at the end of November.

To estimate h_{max} we note that the current version of `bblt` requires a constant value of h_{max} during the simulation and that most of the drilling discharge and our modelling takes place in late October and early November. An estimated surface mixed layer depth of 40 m, yields $h_{max} = 30$ m, based on the 70 m water depth at N. Triumph.

2.7 Drilling Discharge

Estimates of the daily volume of drilling solids discharged from the North Triumph platform were compiled by examination of records from two sources: a spreadsheet provided by the Environmental Effects Monitoring (EEM) contractor, Jacques Whitford Environmental Limited (JWEL), and the records maintained by the drilling mud contractor for the project, MI-SWACO. Daily records of solids discharged were checked against records of volumes shipped. Examination of these records indicated that two discharge scenarios needed to be prepared since there were volume differences of a factor of 3-4 between the two sets of records. The first scenario, based on daily discharge records, is referred to as the "low discharge scenario" and the second, based on total volumes shipped for

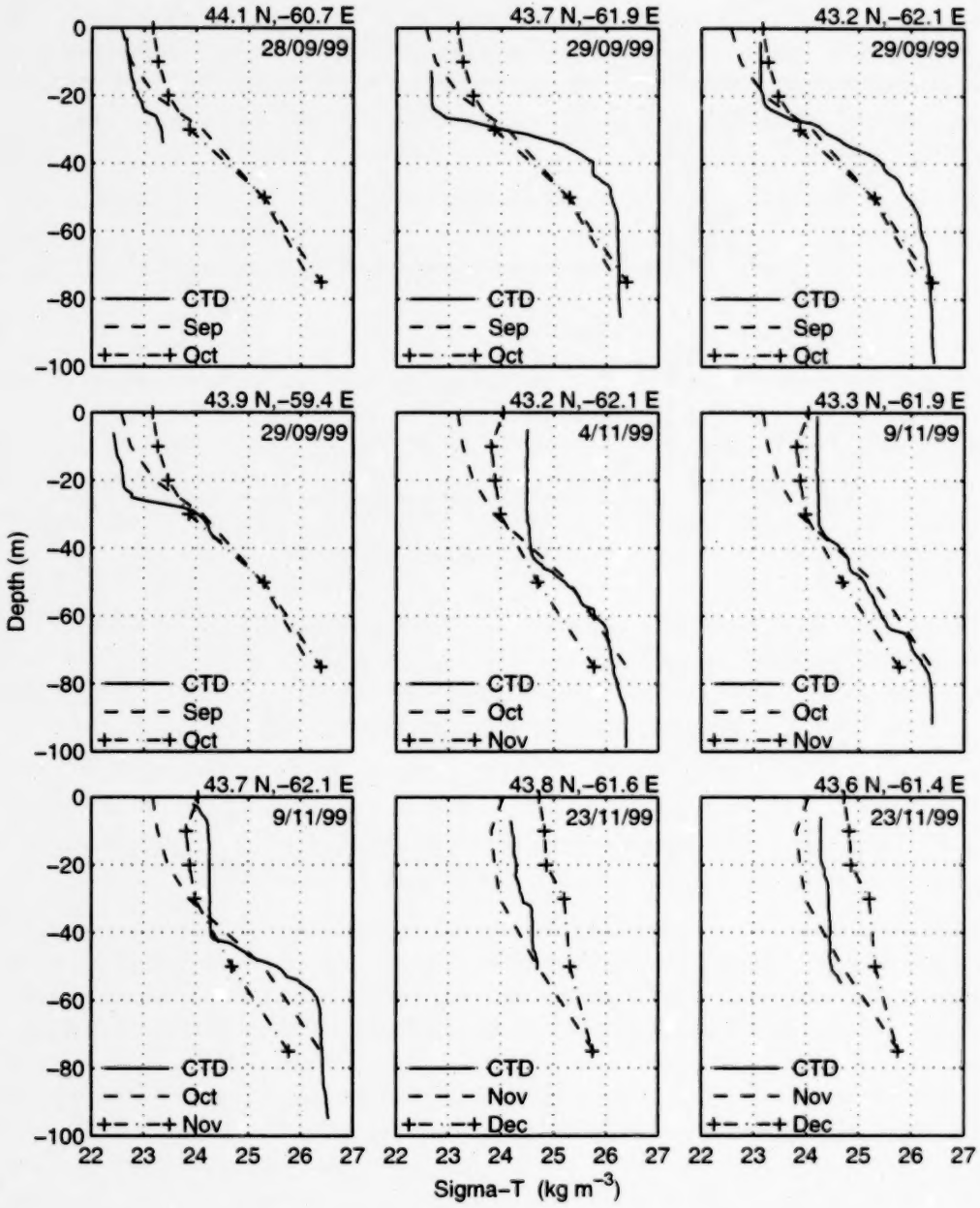

Figure 6: The density profiles used to estimate the boundary layer height h_{max}. The estimate was based on the depth of the surface mixed layer as there are insufficient observations close to the site to infer anything conclusive about the bottom mixed layer heights. The depth of the surface mixed layer for October/November 1999 was estimated to be 40 m. Shown also is the climatology for the months closest to the date of the CTD cast.

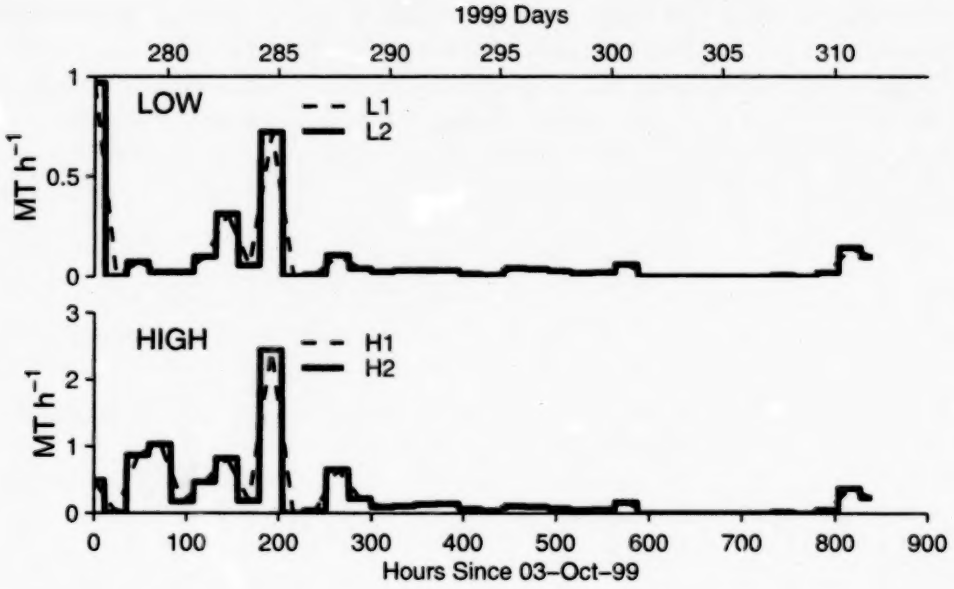

Figure 7: The hourly discharge time series (metric tonnes per hour) for barite derived from the drill logs for North Triumph in the fall of 1999. Low and high discharge scenarios are shown for the two different temporal interpolation schemes: hourly linearly interpolated (L1, H1) and hourly nearest neighbour interpolated (L2, H2). Note that the year day axis is across the top of the plot.

the NT-1 well but apportioned with respect to the discharge fates indicated in the daily records, is referred to as the "high discharge scenario" (Figure 7).

The data obtained from MI-SWACO came from the Daily Mud Reports (DMR), the Mud Volume Accounting (MVA) reports and a Mud Volumes summary. The DMRs provided mud density ($kg\,m^{-3}$) and volume (m^3) data in the following categories: Oil Added, Water Added, Mud Received, Dumped, Shakers, Evaporation, Centrifuge, Formation, Left in Hole, Other. Only the categories of dumped, shakers and centrifuge were relevant to estimating the amount of mud (waste) reaching the environment. Other categories were useful, however, in determining how some of the numbers in the Mud Volumes summary were obtained. The MVA reports presented both "volume balance" and "loss breakdown" information with categories for Dumped, Shakers, Evaporation, Centrifuge, Formation, Left in Hole and Other. For the most part these numbers agree with those in the equivalent categories in the DMRs but where there are discrepancies the MVA figures have been used in our high discharge scenario.

The Mud Volumes summary utilized information from both the DMR and MVA reports and resulted in totals that were approximately twice those provided in the spreadsheet from JWEL. Even so, this did not account for the total volumes of mud that had

been shipped and used, so we prepared the second, high discharge scenario. This scenario was based on the total mud volume shipped and billed, which was then apportioned according to the relative volumes of "surface" (i.e. discharged into the environment) and "subsurface" (i.e. lost to the formation) losses tabulated in MI-SWACO's Mud Volume summary.

The analysis produced daily and cumulative totals for mud volume discharge, density and the particulate barite component. The latter was arrived at from the bulk discharge volume through the following equation:

$$M_{Ba} = V_m(\rho_m - \rho_w)P_{Ba} \tag{2}$$

where V_m is the volume of mud discharged in cubic meters, M_{Ba} is the mass of particulate barite in metric tonnes, ρ_m is the density of the drilling fluid, ρ_w is the density of the seawater in the drilling fluid and P_{Ba} is the proportion of barite in the particulate solids. V_m and ρ_m were obtained from the MI-SWACO records, as described above, ρ_w was obtained from density profile data and P_{Ba} was estimated from MI-SWACO's materials use records and was readjusted for each section of the well based on the proportion of bentonite and barite solids used.

The results of our independent extractions of the barite discharge history for the NT-1 well are shown in Figure 7, with both high and low estimates plotted using two interpolation schemes. The high discharge scenarios (H1 and H2) contain 212 tonnes of barite, while the low scenarios (L1 and L2) contain 60 tonnes, reflecting a large uncertainty in the discharge volumes

2.8 EEM Program Sampling

JWEL was contracted by Sable Island Energy Inc. (SOEI) to conduct an EEM sampling program with baseline and subsequent operational phases. At North Triumph the baseline sampling was carried out in mid June, 1999, prior to spudding well NT-1. The only operational phase EEM sampling carried out at this site, during the period in which drilling muds were being discharged (which ended 31, December, 1999), was conducted from October 28 through November 5, 1999 (SOEI, 2000). The timing of the sampling relative to the discharge and other observational data is shown in Figure 3.

The two aspects of the EEM sampling program relevant to detecting barite concentrations were bottom sediment sampling and sampling of water and suspended particulate matter at 0.5 m above the seabed. The former was accomplished with a Smith-McIntyre grab, while the suspended samples were obtained with a device based on the CABLE sampler (Compact Aquatic Boundary Layer Explorer) developed at BIO (Milligan et al., 1998). The device combines optical and direct sampling devices. Water sampled directly was filtered, dried and weighed to determine total SPM before being sent out for barium analysis.

The sampling grid and the observed concentrations from the Oct/Nov 1999 EEM program are given in Table 3 and Figure 8. The measured barium ion concentrations have been converted to barite concentrations by multiplying the barium ion value by 1.7, as barium ion comprises 59% of the barite ($BaSO_4$) molecule by weight. Inspection of Figure 8 reveals no obvious patterns in terms of distance from the rig, but does suggest larger concentrations to the north.

The effective barite concentrations, with values typically $< 1\ \mu g\,L^{-1}$, are small relative to the 100 $\mu g\,L^{-1}$ (0.1 $mg\,L^{-1}$) level of the no effects concentration for scallops that Gordon et al. (2000) inferred from the laboratory experiments of Cranford et al. (1999). In fact, the values are so small that we need to be concerned about what the background levels of barite are, as `bblt` can only be expected to model the concentrations due to the October 1999 discharges. Concentrations due to naturally occurring barite in the suspended sediment and due to previous drilling activities must be removed before comparison with the `bblt` simulations.

Barium and barite occur naturally in both the water column and the sediment. For example, IAPSO standard sea water contains barium concentration in the range 4-20 mg kg^{-1} (or $\mu g\,L^{-1}$) (from the web page of Ocean Scientific International Limited, www.osil.co.uk, the official supplier of IAPSO standard sea water). This dissolved material should not directly impact the measurements of barium in the suspended particulate matter (SPM) but phytoplankton uptake of barium and barite may contribute to the background levels of barium in the SPM.

The natural levels of barium (in the form of barite) in the sediment are estimated to be 50 - 260 mg kg^{-1} (the units here are per kg of sediment). This was estimated from the Fall 1999 EEM sediment data using the co-incident aluminium measurements as a normalization. Based on this, the barium concentrations in the range 580 - 1900 mg kg^{-1} measured at four of the 500 m stations represent elevated levels of barium (barite). The levels of barium in the SPM are in the range 500 - 1500 mg kg^{-1} consistent with the idea that higher barium (and other metals) levels are associated with the smaller sediment size fraction (Phil Yeats, BIO, pers. comm. 2003).

Given the low measured concentrations, we also need to be concerned with detection limits. From the SOEI EEM data at N. Triumph the detection limits for barium were 0.3 $\mu g\,L^{-1}$ in 1998, 0.2 $\mu g\,L^{-1}$ in 1999, and essentially zero for our purposes in 2000. As a measure of variability we note that over the 5 EEM observation periods at N. Triumph (1998 through 2000), the field duplicates typically vary by less than 0.2 $\mu g\,L^{-1}$, but in two cases varied by 1 $\mu g\,L^{-1}$ which is our signal level.

The issue of the appropriate background barite value will be addressed in Section 3.2.

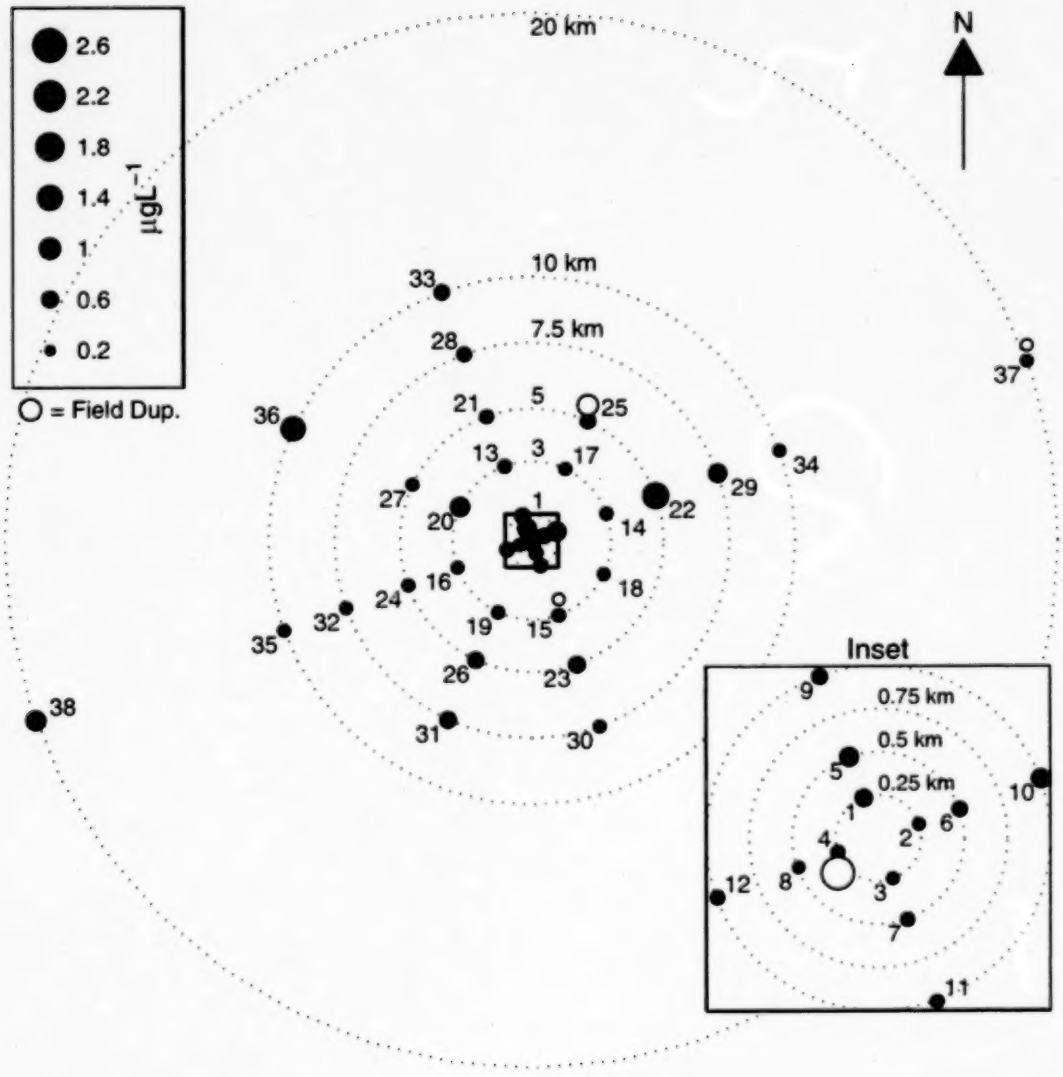

Figure 8: The location map of the suspended barite observations taken over the period 28 Oct. to 5 Nov. 1999. The barium concentration is shown with expanding circles, the area is proportional to concentration (duplicate samples shown with an open circle). The sample location ID numbers are shown next to the observations. The barium concentrations have been converted to barite as described in the text.

Table 3: Observations of suspended barium and barite concentrations at locations relative to rig. Samples were taken at 0.5 mab. The sample locations are referenced by ID number in Figure 8. The samples labelled JWDup are duplicate water samples taken at the same location. The barium concentrations were converted to barite as described in the text.

ID	East (km)	North (km)	Name	Barium($\mu g\,L^{-1}$)	Barite($\mu g\,L^{-1}$)
1	-0.084	0.233	NT-250-1-D3	0.4	0.680
2	0.236	0.082	NT-250-3-D3	<0.2	<0.340
3	0.085	-0.232	NT-250-5-D3	<0.2	<0.340
4	-0.235	-0.081	NT-250-7-D3	0.25	0.425
			JWDup	1.55	2.635
5	-0.169	0.471	NT-500-1-D3	0.47	0.799
6	0.472	0.169	NT-500-3-D3	0.3	0.510
7	0.170	-0.470	NT-500-5-D3	0.25	0.425
8	-0.463	-0.168	NT-500-7-D3	<0.2	<0.340
9	-0.338	0.936	NT-1000-1-D3	<0.32	<0.544
10	0.942	0.343	NT-1000-3-D3	0.47	0.799
11	0.340	-0.947	NT-1000-5-D3	0.24	0.408
12	-0.933	-0.342	NT-1000-7-D3	0.27	0.459
13	-1.016	2.818	NT-3000-1-D3	0.23	0.391
14	2.818	1.016	NT-3000-3-D3	0.22	0.374
15	1.019	-2.829	NT-3000-5-D3	0.23	0.391
			JWDup	<0.2	<0.340
16	-2.810	-1.014	NT-3000-7-D3	<0.2	<0.340
17	1.277	2.715	NT-3000-2-D3	<0.2	<0.340
18	2.715	-1.277	NT-3000-4-D3	<0.2	<0.340
19	-1.277	-2.715	NT-3000-6-D3	<0.21	<0.357
20	-2.715	1.277	NT-3000-8-D3	0.48	0.816
21	-1.694	4.701	NT-5000-1-D3	0.23	0.391
22	4.693	1.690	NT-5000-3-D3	0.9	1.530
23	1.697	-4.700	NT-5000-5-D3	0.35	0.595
24	-4.687	-1.686	NT-5000-7-D3	<0.2	<0.340
25	2.128	4.524	NT-5000-2-D3	0.3	0.510
			JWDup	0.6	1.020
26	-2.128	-4.524	NT-5000-6-D3	0.33	0.561
27	-4.524	2.128	NT-5000-8-D3	<0.2	<0.340

... Table 3 Continued

ID	East (km)	North (km)	Name	Barium($\mu g\,L^{-1}$)	Barite($\mu g\,L^{-1}$)
28	-2.542	7.056	NT-7500-1-D3	0.27	0.459
29	7.056	2.542	NT-7500-3-D3	0.44	0.748
30	2.542	-7.056	NT-7500-5-D3	0.2	0.340
31	-3.192	-6.787	NT-7500-6-D3	0.35	0.595
32	-7.056	-2.542	NT-7500-7-D3	<0.2	<0.340
33	-3.389	9.408	NT-10000-1-D3	0.3	0.510
34	9.408	3.389	NT-10000-3-D3	<0.2	<0.340
35	-9.408	-3.389	NT-10000-7-D3	<0.2	<0.340
36	-9.049	4.257	NT-10000-8-D3	0.77	1.309
37	18.817	6.777	NT-20000-3-D3	<0.2	<0.340
			JW-Dup	<0.2	<0.340
38	-18.817	-6.777	NT-20000-7-D3	0.5	0.850

Table 4: Parameter values used for `bblt` runs.

Parameter	**Value**
Vertical Shuffling Time (t_m)	3.0 hours
Advection Time Step (Δt_a)	0.1 hours
Simulation Period	900 hours
Current meter time interval	1.0 hour
Reference Height (h_{ref})	0.0035 m
Boundary Layer Height (h_{max})	30 m

2.9 `bblt` Simulations

The simulation and analysis procedure was designed to compensate for the fact that the discharges are known only approximately and the currents are not known for the 9 days prior to and during the EEM observations. The basic set of model runs consists of 40 simulations: the 4 discharge scenarios, each run with the 10 different realizations of the currents and bottom stress. Each simulation started on 3 Oct. 1999 and ran through 9 Nov. 1999 (900 hours). In the analysis each simulation is treated as being equally likely. As a sensitivity study, runs were also done with the discharges shifted ahead and behind by one day relative to the currents. Given the coarse comparison with the observation, these runs did not contribute any new information to the discussion and the results are not reported here. The basic `bblt` parameters are listed in Table 4.

During each run the concentrations at the EEM sites were recorded hourly at 0.5 mab (actually the average concentration between 0.45 and 0.55 mab) and at the near-bottom (the average over the bottom 10 cm). In addition, near-bottom concentrations

were sampled on a 400 m regular grid covering the 12 x 12 km region around the rig.

In addition to the stress-dependent settling velocity, another set of 40 simulations was performed using a constant settling velocity $w_1 = 0.1$ cm s^{-1}and u_{*c} for the friction velocity. These simulations address the issue of he sensitivity of the concentrations to basic model assumptions.

A feature of the new 3D (volumetric) concentration calculation (Section 2.1) is that the minimum resolvable concentration (due to 1 particle) is not a constant. It depends on the vertical position in the water column, the vertical distribution of the material and the minimum single particle depth-integrated concentration determined by particle mass and radius of the sampling cylinder. The minimum bottom concentration (C_{Bmin}) is a constant and provides an upper bound on the minimum concentration values in the water column. This upper bound is achieved when the distribution is vertically uniform (high bottom stress / low Rouse number) and is computed by dividing the minimum depth-integrated concentration by h_{max}. The number of particles and radius of the sampling cylinder were chosen to yield a C_{Bmin} value well below the EEM observations. The cylinder radius was 250 m and we used 600,000 particles for H1 and H2 (212 tonnes) and 200,000 particles for L1 and L2 (60 tonnes). The C_{Bmin} was 0.06 μg L^{-1} for H1 and H2 and 0.05 μg L^{-1} for L1 and L2. For the near-bottom concentrations on the grid, the 400 m grid resolution was chosen to yield C_{Bmin} similar to those at the EEM sites.

3 Results

The results are divided into four parts. The first is concerned with the bottom stress time series and its implications for the settling velocity. The second addresses the issue of background barium/barite concentration. The third part is a comparison of the simulated and observed barite concentrations at 0.5 mab. The last is a presentation of the near-bottom concentrations over the entire discharge period.

3.1 Bottom Stress and Median Height

The total friction velocity u_{*cw} is large relative to the critical value for floc breakup u_*^c = 1.0 cm s^{-1} (Figure 4). Therefore in the stress-dependent settling velocity model, the flocs do not maintain their initial settling velocity (w_0) for very long. Figure 9 shows that the survival time for the initial flocs is 1 hour or less (1 model time step) about 65% of the time and less than 9 hours 99% of the time. Thereafter the flocs flip back and forth between the natural marine floc (w_1) and the broken-state (w_2). The short survival time of the initial flocs makes the alternate settling velocity scenario (constant settling velocity) a reasonable one.

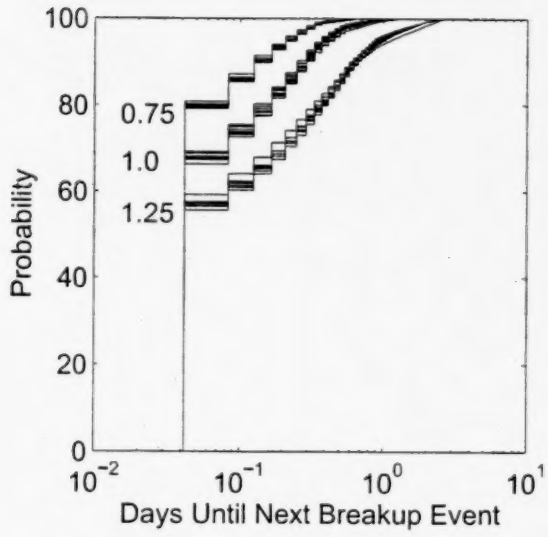

Figure 9: The probability(%) of breakup occurring before X days. Results are shown for three different critical stresses $u_*^c = 0.75$, 1.0 and 1.25 $\mathrm{cm\,s^{-1}}$. Superimposed are curves calculated from the 10 versions of the synthetic currents.

Figure 10 shows the median height time series for fall 1999. The calculation accounts for the continuous discharge and stress-dependent settling velocity. The primary result is that the sediment is uniformly distributed in the vertical (median height $\approx$ 15 m) about 70% of the time. There is a small seasonal evolution from 64% in Oct. to 72% in Nov. and 76% in Dec. For the constant settling (and u_{*c}) case, the median height does not exceed 14 m and is less than 12 m approximately 50% of the time with no significant seasonal variability.

3.2 The EEM Data

Visual inspection of the suspended barium data from June 1999 and the fall of 1999 suggests that the background level of barium is 0.3-0.5 $\mu\mathrm{g\,L^{-1}}$ (Figure 11), but it could be as much as 0.6 $\mu\mathrm{g\,L^{-1}}$. The median value of the observations is close to the detection limit of 0.2 $\mu\mathrm{g\,L^{-1}}$.

These background values are not necessarily the pristine background, rather they represent the background for the vicinity of N. Triumph given the natural barium concentrations in the sediment and the seawater plus any residual barium from previous drilling activity. It is the appropriate background for comparing `bblt` output with the observations. It may not be appropriate for determining long term accumulations.

There are several interesting points to be made about the observations.

- The highest concentration in the June 1999 observations is 20 km from the rig. It is certainly not due to the drilling at N. Triumph in the fall of 1999. It may be due

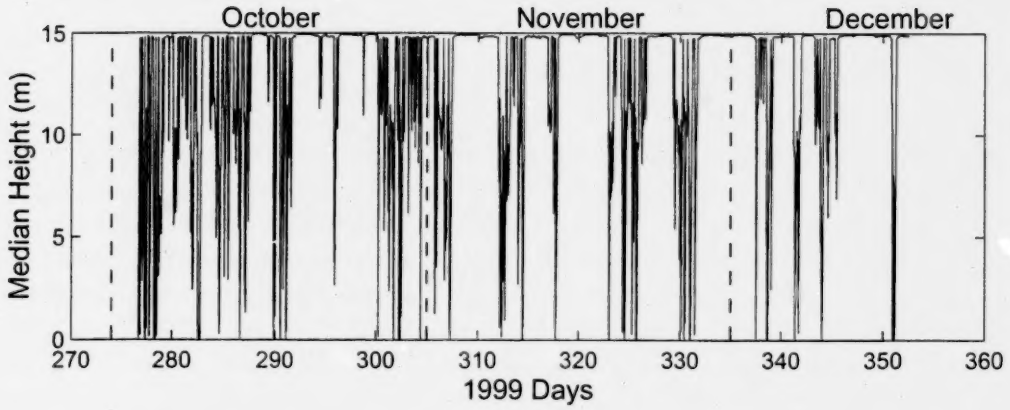

Figure 10: Median sediment height derived from the Rouse profile. The calculation included break up (u_*^c=1.0 cm s^{-1}) as well the continuous discharge time series for computing the fraction of initial (heavy) and natural (light) flocs.

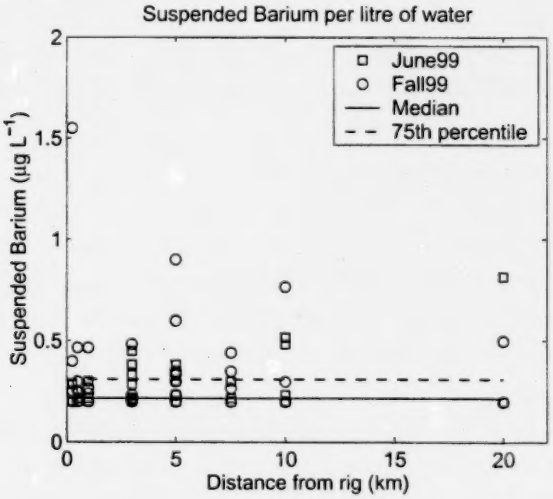

Figure 11: The suspended barium concentration data from the EEM program as a function of the distance from the rig. Data is shown for the background cruise in June 1999 and the EEM cruise in Oct/Nov 1999. There is a background barium concentration of 0.3-0.5 μg L^{-1}. Above this background there is an apparent signal decaying away from the rig.

to drilling at Venture or Thebaud in the spring of 1999.

- For the fall of 1999, the maximum values at distances of 250 m, 5 km, 10 km and 20 km show a smooth decay away from the rig.

- A possible interpretation of Figure 11 is that proper background value is 0.6 $\mu g\, L^{-1}$ and that only 3 values are above background.

As a first cut we will use a background barite concentration of 0.42 $\mu g\, L^{-1}$(equivalent to 0.25 $\mu g\, L^{-1}$ of barium). We will revisit this in the discussion. The background barite concentration will be subtracted from the observations and all resultant concentrations less than 0 will be set to 0.

3.3 Comparison With EEM Data

The basics of the simulations are illustrated in Figure 12. This shows the timing of the discharges, the EEM observations, the real and synthetic currents, and the simulated concentrations close to the rig. Notice that the EEM program occurs about 15 days after the peak discharges and about 9 days after the velocity observations end. The reader should also note that the EEM measurements were made during a period of no discharges and that the simulated concentrations decrease rapidly (by at least two orders of magnitude) during the first two days of the EEM program. Also note that the dates when the individual EEM samples were taken are not available.

The simulated concentrations at 4 locations are shown in Figure 13. The locations are at 250 m, 500 m, 1000 m, and 3000 m from the rig (top to bottom). Overall, the concentrations decrease with distance, but the basic features of the concentration time series are similar at the different locations. Notice that the simulated concentrations are zero for much of the EEM observation period.

The simulated concentrations have reduced variability during the period of synthetic currents than during the period of the real ADCP data. This is because during the period of the synthetic currents the mean over the 10 different realizations is shown. The range of variability is indicated by the dashed line representing the maximum of the 10 simulations. The minimum at any time is usually zero. The small amount of variability due to differences in the vertical shuffling scheme induced by the different random number sequences used for the different simulations is illustrated by the occasional appearance of the red dashed line indicating the maximum value during the period of the real ADCP data.

Figure 14 shows the predicted probability of occurrence of different concentration levels at 0.5 mab for the observation locations during for the observation period. The most striking feature is the dominance of the lowest concentration values: zero is a

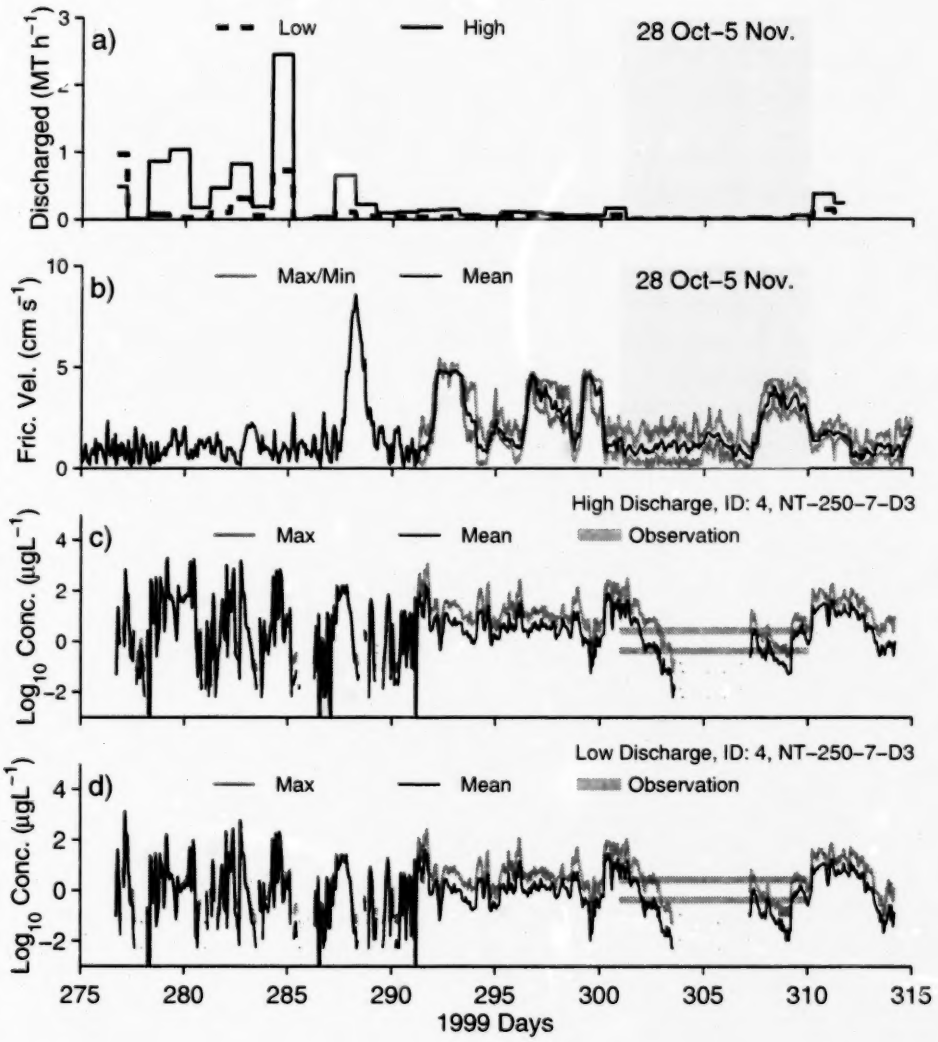

Figure 12: The timing of the discharges and the EEM program in relation to the simulated concentrations close to the rig. Panel a) shows the high (H2) and low (L2) discharges. Panel b) shows the friction velocity (u_{*cw}) and the timing of the real and synthetic currents. The period of the synthetic currents is indicated by the maximum and minimum values of u_{*cw} (dashed red lines). Panels c) and d) show the simulated barite concentrations for H2 and L2 at 0.5 mab at an observation location 250 m from the rig. The mean (over the 10 realizations of the currents) and maximum simulated concentrations are shown. The minimum concentrations are frequently zero and are not shown. The observed barite concentrations are shown by the horizontal grey bars whose length indicates the timing of the EEM program. Duplicate measurements were made at this location.

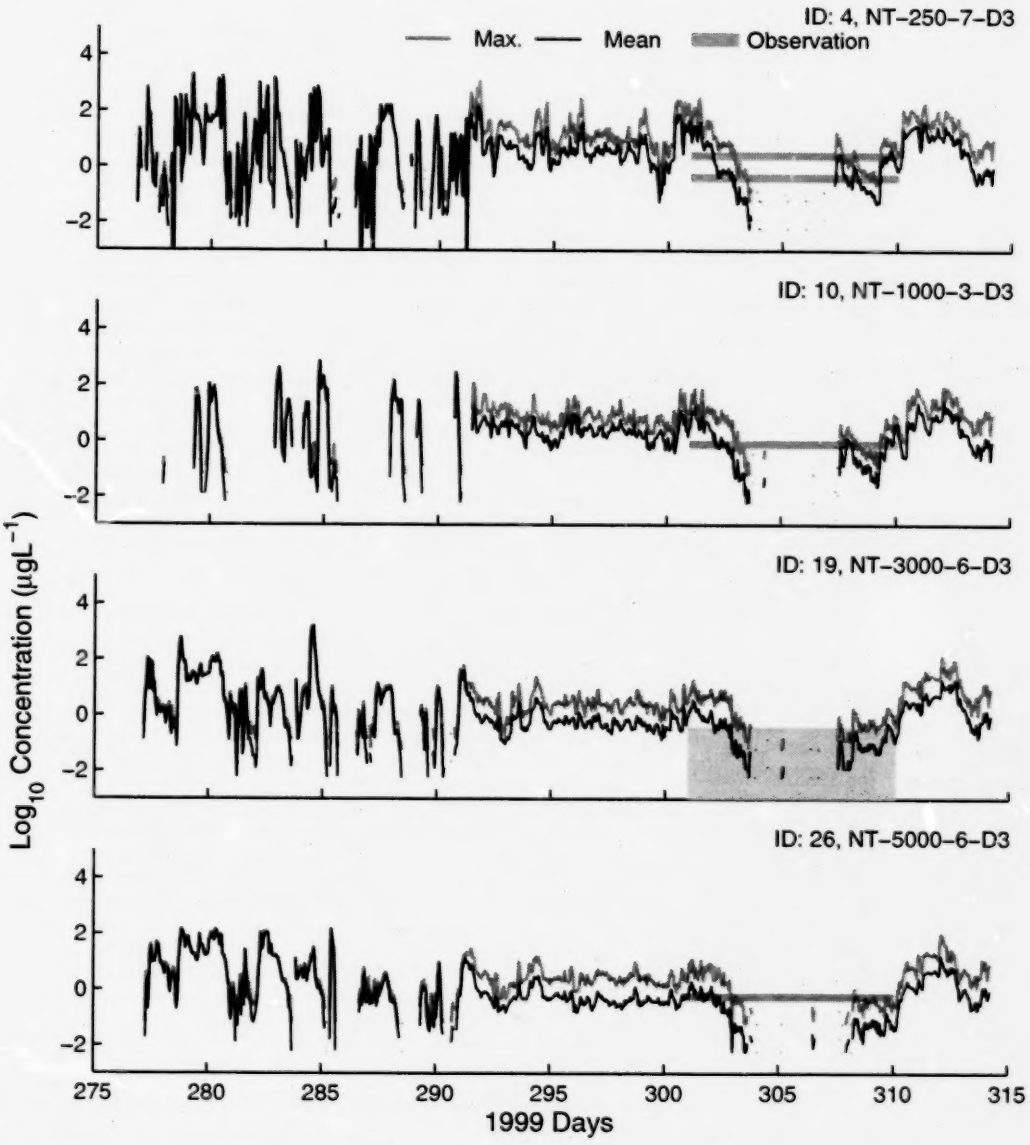

Figure 13: Concentration of barite at 0.5 mab for observation locations 4, 10, 19 and 26 (refer to Figure 8). The distance from the rig is coded in the site name. Shown are the mean (black) and maximum (dashed red) concentrations from the 10 synthetic time series using discharge H2. The occasional deviation of the mean and maximum during the period of real current data (days 277 to 291) indicates the variability due to the vertical mixing. Shaded region indicates the time at which field observations were taken (28 Oct. to 5 Nov. 1999) and the measured barite concentrations (Table 3).

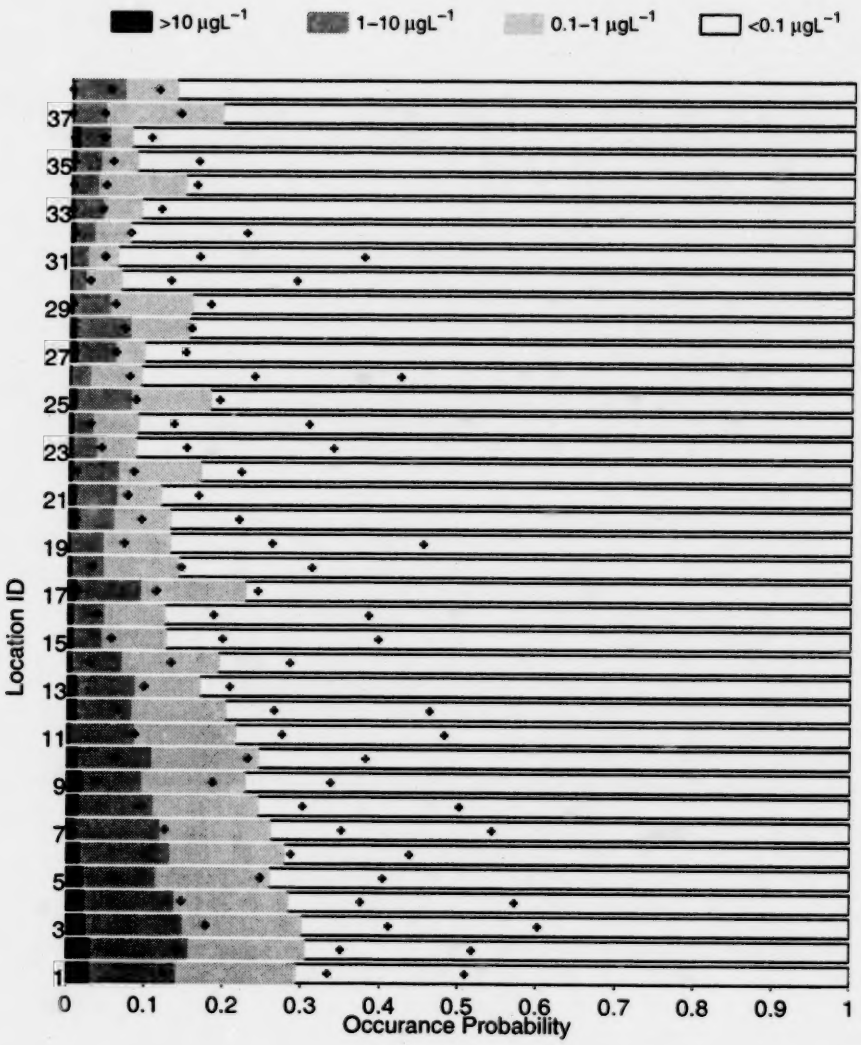

Figure 14: Predicted probability of the occurrence of different barite concentration levels at 0.5 mab for the observation locations. The locations are ordered by Location ID. In general the smaller numbers are closer to the rig than the larger ones (Figure. 8). There is a general decrease in the occurrence of large concentrations with distance from the rig, but there are exceptions (e.g. ID 17, 25, 29, 37). The probability was computed using the 40 basic runs with the stress-dependent settling velocity. The shaded bars show the results for the EEM period. The results for the entire simulation, shown using the +, depict the increased occurrence of the high concentrations due to the large discharge early in the simulation period.

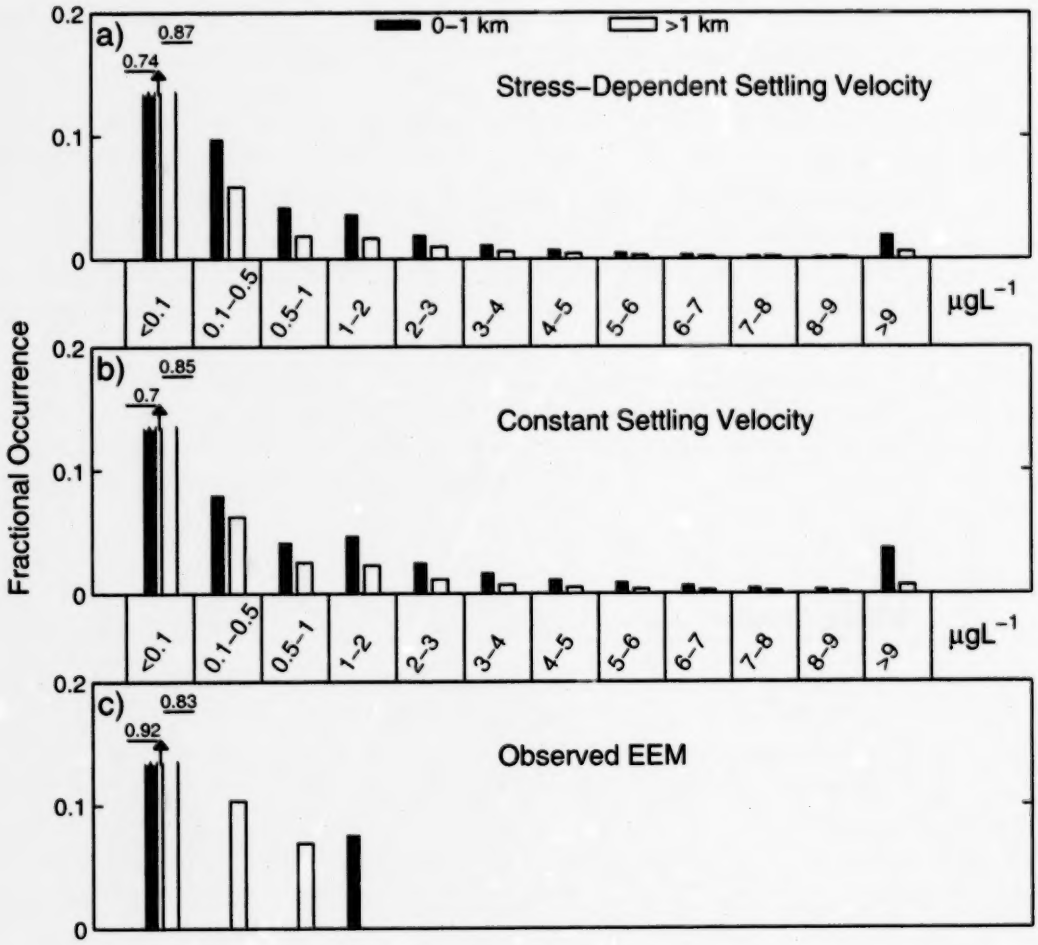

Figure 15: Comparison of frequency of occurrence of different barite concentration levels during the EEM period 28 Oct. to 5 Nov. 1999. Concentrations were calculated at 0.5 mab for all EEM observation locations. Panel a) shows the results for the stress-dependent settling velocity; b) the results for the constant settling velocity; and c) the EEM observations with the background value of 0.425 $\mu g\, L^{-1}$ subtracted. The results have been separated into locations near the rig ($\leq$ 1 km) and further from the rig ($>$ 1 km) to provide some spatial information.

common value. There is a general decrease in the occurrence of large concentrations with distance from the rig, but there are exceptions (e.g. ID 17, 25, 29, 37).

The fact that we don't know the currents for the 10 days or so before the EEM period makes it problematic to compare the observations and the simulations on a point by point basis. A second complication is the dramatic reduction in the simulated concentrations

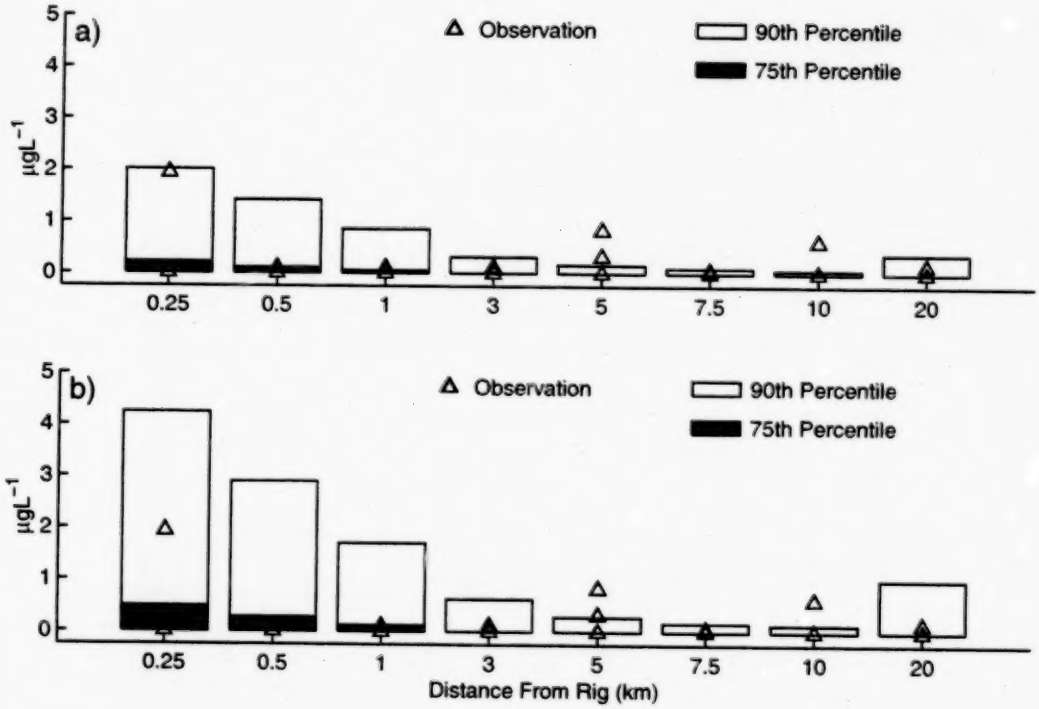

Figure 16: Concentration as a function of distance from rig. The observations are shown as $\triangle$. The simulated results are shown for the 75th and 90th percentiles computed over the 40 basic simulations for a) the stress-dependent settling velocity and b) the constant settling velocity case. The background value was removed from the observation. The results for constant settling velocity were similar to the stress-dependent settling velocity case except that the 75th and 90th percentiles were about a factor of 2 larger.

during the first two days of the EEM program. Small differences in timing could cause large differences in concentration.

For the first overall comparison we simply compare all the observed concentrations (with the background removed) to all the simulated concentrations during the EEM period. Figure 15 shows the frequency of occurrence of different concentration levels at the survey sites during the EEM period. The only spatial information is the separation of the regions ≤ 1 km from those > 1 km from the rig. The results indicate a general agreement about the overall level of the concentrations and show the dominance of very small values.

For the second comparison we consider the simulated and observed concentrations as a function of distance from the rig (Figure 16). There is general agreement in that the concentrations are very low and that zeroes are often observed. In addition, the largest concentration value is found nearest the rig. It is encouraging that the observations

generally fall inside the 90th percentile of the model results. The exceptions are at 5, 7.5 and 10 km from the rig. The simulated concentrations decay smoothly away from the rig, except for an increase at 20 km. The observations could be interpreted to decay smoothly away from the rig with either anomalously high values at 5, 7.5 and 10 km or anomalously low values at 0.5, 1, and 3 km.

Three final points. Firstly, all the observations except the 3 largest (at 0.25, 5, and 10 km) could be background values. Secondly, the simulations show that the concentrations can vary rapidly on time scales shorter than the EEM observation period. Thus interpreting the observations as a snapshot of the concentration field is potentially misleading. Finally, in the simulations anomalously large concentrations can suddenly appear at some distance from the rig if the friction velocity decreases and the sediment settles into the near-bottom. It is only in the average that a smooth distribution appears. In these simulations it appears that at least one currents/stress time series resulted in anomalous concentrations at a site 20 km from the rig.

3.4 Near-bottom Concentration

The time series of near-bottom concentration (Figure 17) have the same general features as the 0.5 mab time series. The concentrations are simply a bit larger.

As a measure of the overall levels of near-bottom concentration and exposure of near-bottom organisms to barite from drilling mud, we consider the total time that a given location experiences concentrations above a particular level. Figure 18 shows the results for the stress-dependent settling settling velocity during the EEM period and Figures 19 and 20 the results during the entire simulation period. The most important feature is the two order of magnitude change in the concentration levels chosen for these two periods. The difference in overall exposure levels is consistent with the concentration time series shown in Figure 17; the concentrations are much lower during the EEM period than in the earlier period.

A second important difference between the exposure plots is that during the EEM period the simulations indicate a mean drift to the northeast (Figure 18) while the mean drift is to the southwest over the entire simulation (Figures 19 and 20). The difference is due to the differences between the observed currents and the synthetic currents in the data gap. The observed currents show a mean drift to the southwest. During the EEM period the synthetic currents have the feature that 8 of 10 realizations showed mean drift to the north during the EEM period. This seems to be a chance result of the statistical procedure used to construct the synthetic currents. We did not force the mean to agree with that from the ADCP observations. The difference in the mean reinforces the idea that the currents leading up to the EEM observations are unknown.

Figures 21 and 22 show the exposure maps for the constant settling velocity case

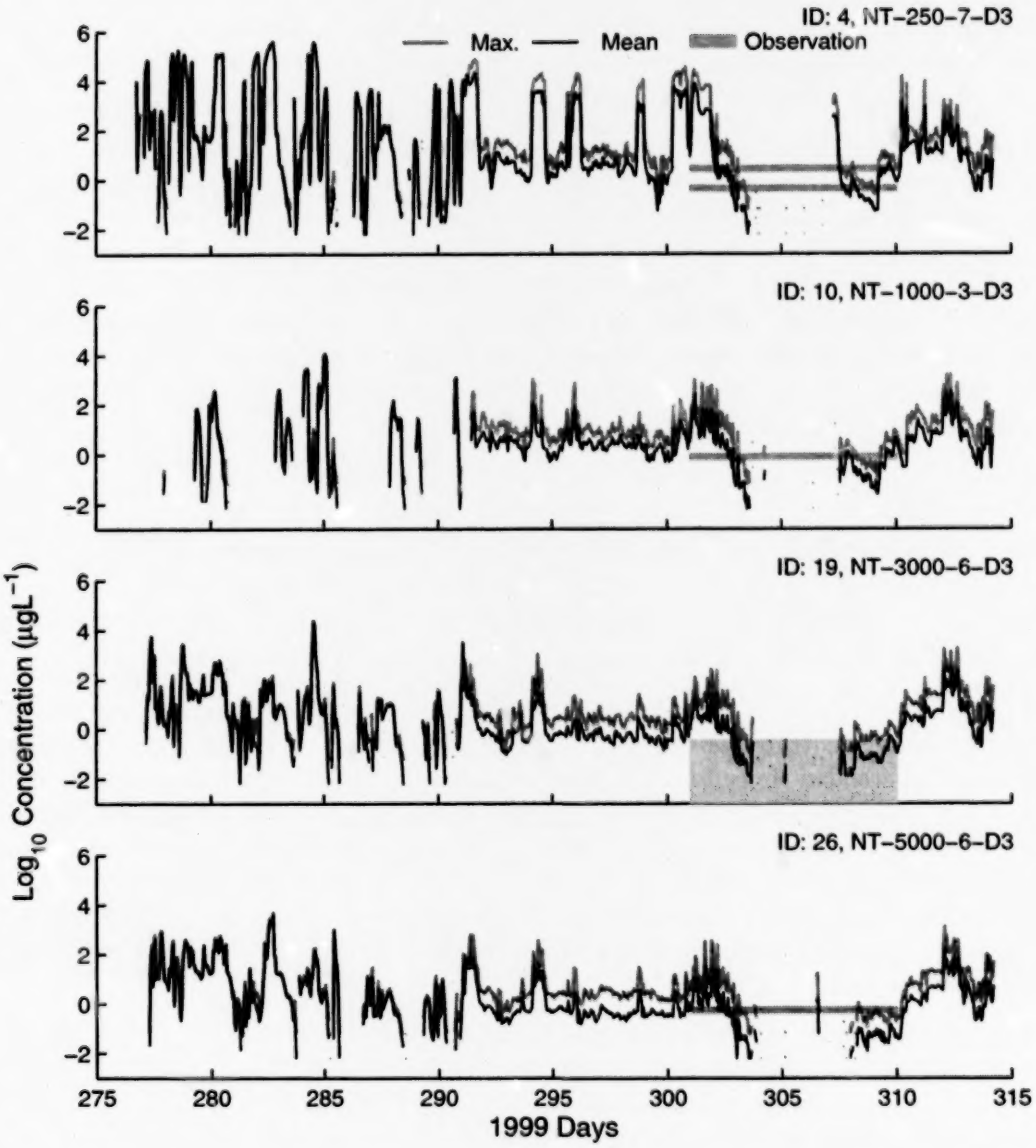

Figure 17: Near-bottom concentration of barite at selected observation locations. Shown are the mean and maximum values from the 10 basic runs with the stress-dependent settling velocity and the discharge time series H2. The observations at 0.5 mab are shown in the same fashion as previous figures. The shaded regions show observed concentrations of barite for the period 28 Oct. to 5 Nov. 1999 (Table 3).

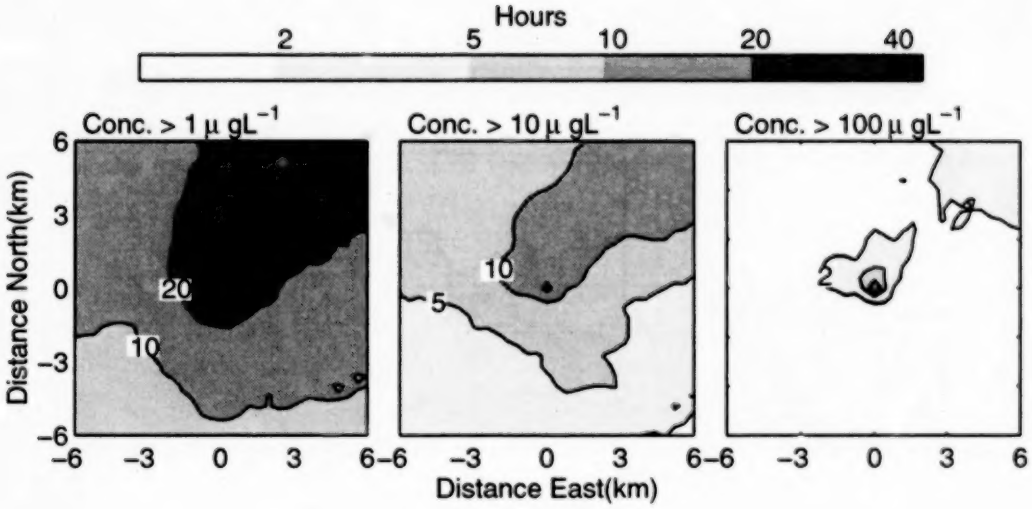

Figure 18: Map of time (hours) that the near-bottom barite concentration was above 1.0, 10 and 100 μg L^{-1} for 28 Oct. to 5 Nov. 1999. The results for H1 and H2 discharges were averaged over the 20 simulations with the stress-dependent settling velocity. The simulations with L1 and L2 discharges had the same spatial pattern but the exposure time was about 1/2 the values shown here.

with the high and low discharge estimates. The overall spatial patterns and the exposure times are similar to Figures 19 and 20.

Figure 23 shows the variability in the exposure time for the stress-dependent high discharge case. This variability is the maximum difference from the mean computed from among the 20 simulations. The variability at distances >1 km from the rig is small (<15 hours). However over much of the region the mean exposure time (Figure 19) and the variation are the same order of magnitude.

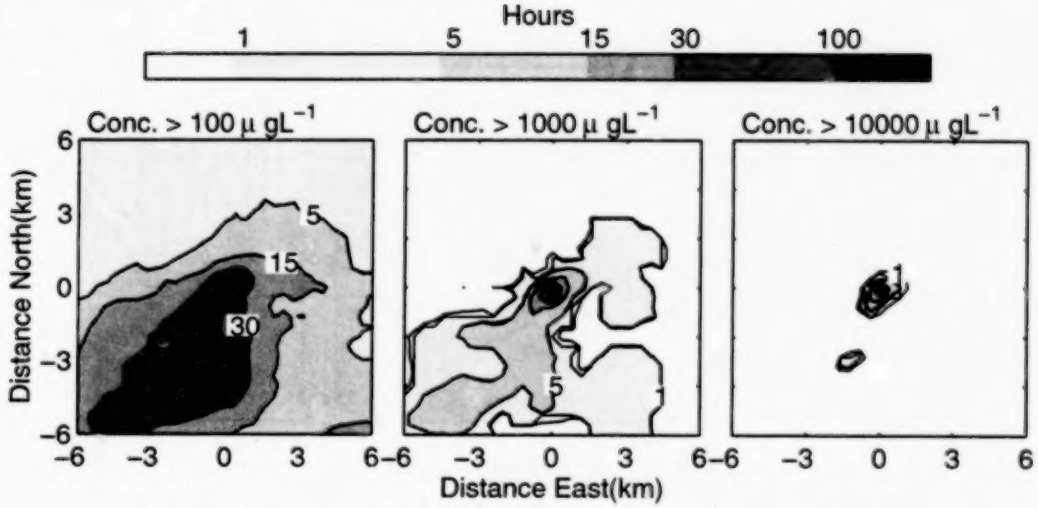

Figure 19: The total time (hours) during the entire simulation (900 h), within which the near-bottom barite concentration was above 100, 1000 and 10000 $\mu g\,L^{-1}$ for the stress-dependent settling velocity case. The results here are the average of the 20 simulations for the H1 and H2 discharges. The no effects concentration for scallops has been estimated at 100 $\mu g\,L^{-1}$.

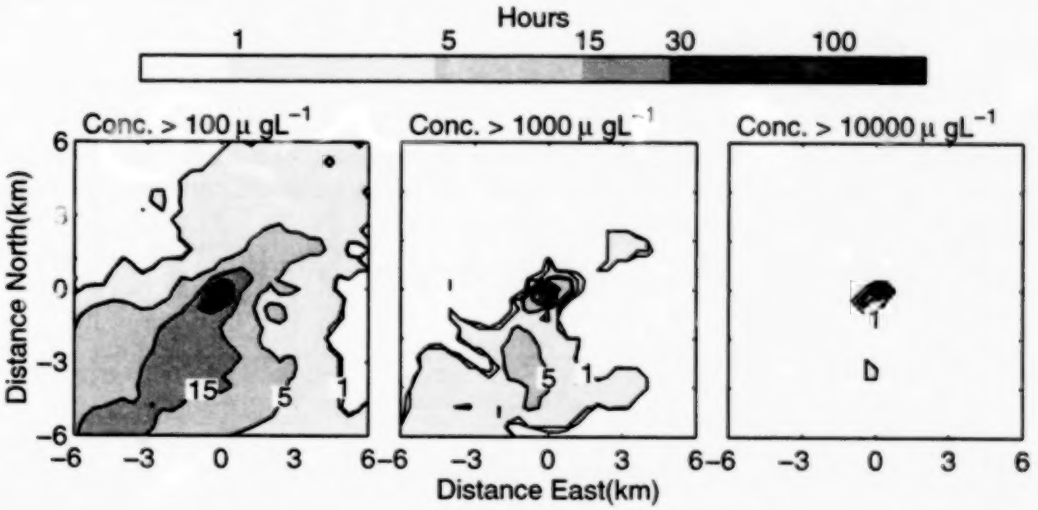

Figure 20: The total time (hours) during the entire simulation (900 h) within which the near-bottom barite concentration was above 100, 1000 and 10000 $\mu g\,L^{-1}$ for the stress-dependent settling velocity case. The results here are the average of the 20 simulations for the L1 and L2 discharges.

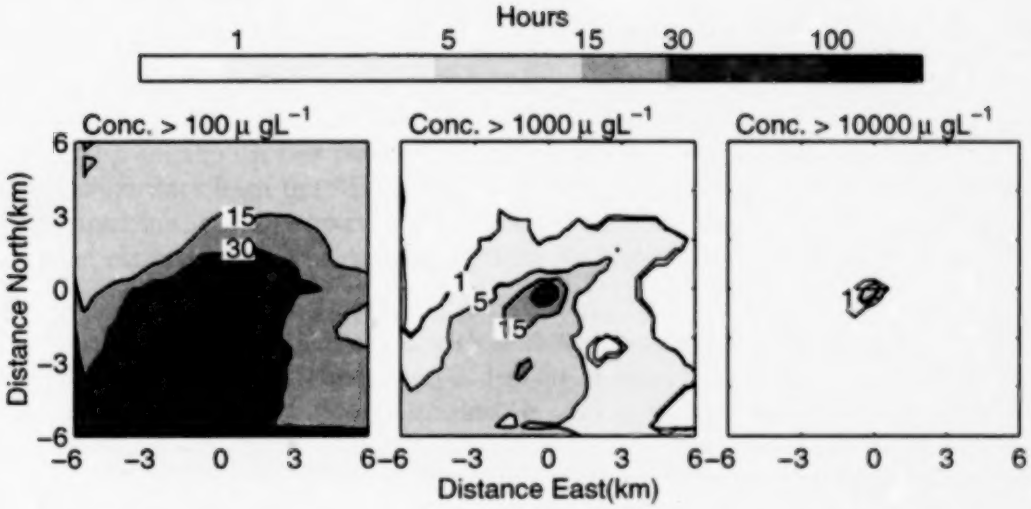

Figure 21: The total time (hours) during the entire simulation (900 h) within which the near-bottom barite concentration was above 100, 1000 and 10000 μg L^{-1} for the constant settling velocity case. The results here are the average of the 20 simulations for the H1 and H2 discharges.

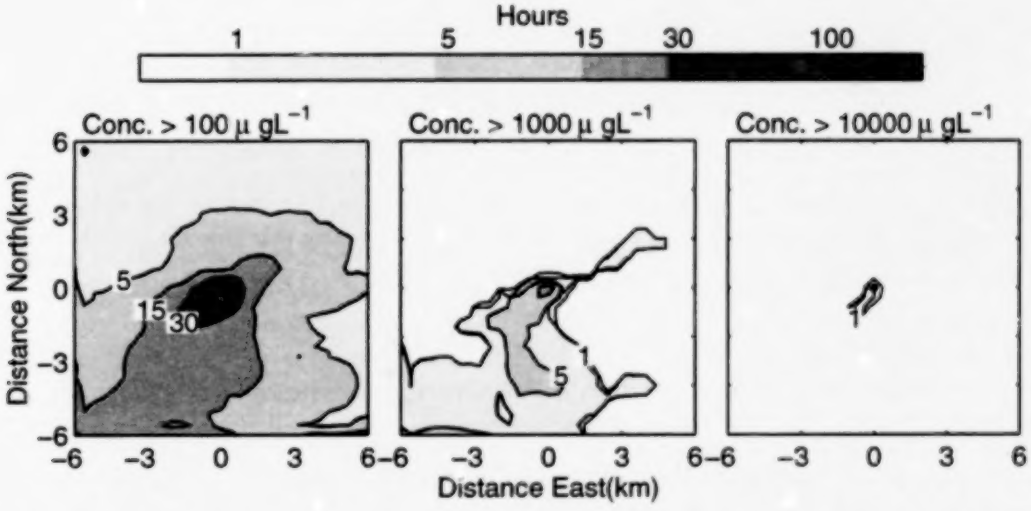

Figure 22: The total time (hours) during the entire simulation (900 h) within which the near-bottom barite concentration was above 100, 1000 and 10000 μg L^{-1} for the constant settling velocity case. The results here are the average of the 20 simulations for the L1 and L2 discharges.

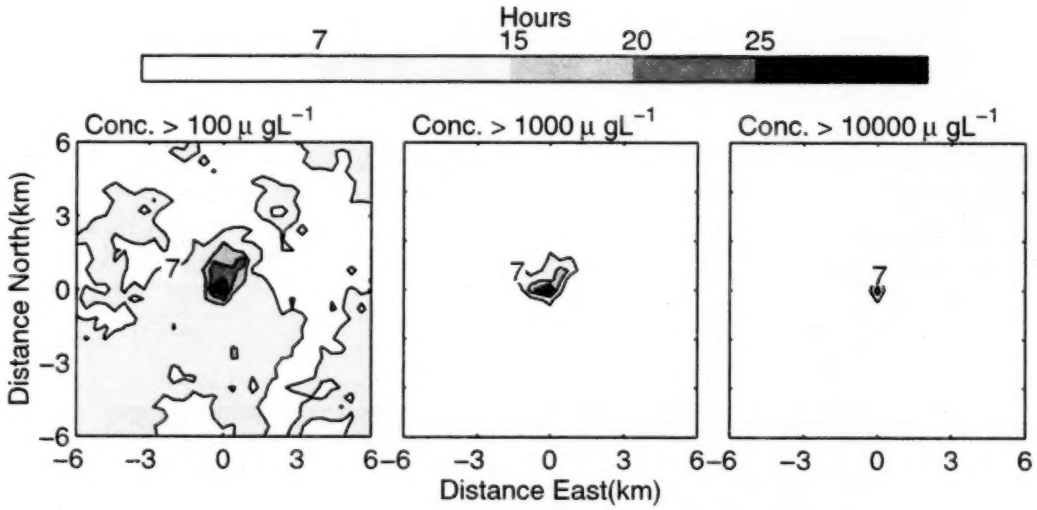

Figure 23: Variability in exposure time (hours) over the 20 runs for the entire period with stress-dependent settling and high discharge. Variability was taken as the maximum deviation from the mean.

4 Discussion

The barite concentrations due to the drilling activity at North Triumph in the fall of 1999 were estimated using the `bblt` model. The simulations used discharge time series estimated from the drilling records, currents from the local ADCP measurements and surface wave data from the AES40 wave hindcast. The currents data did not cover the 9 days prior to the EEM observations or the period of the observations. Currents in this gap were estimated using statistical methods to generate an ensemble of 10 synthetic current time series.

The simulations were performed with both a stress-dependent settling velocity and a constant settling velocity. For the stress-dependent case, the high friction velocity causes rapid breakup of the dense flocs (with the fast settling velocity w_0). After discharge, 65% of the dense flocs break up within an hour and 99% are broken up within 9 hours. This results in a near constant settling velocity with the very slow velocity (w_2). On the other hand barite is a mineral grain and will not break up under high stress. The constant settling velocity scenario (with settling velocity 0.1 $\mathrm{cm\,s^{-1}}$) assumes that the dense flocs are broken up and that the barite is transported as single grains. The very short survival time for the dense flocs is very different from the findings of Tedford et al. (2002, 2003) for Hibernia, where a dense floc had a 50% chance of surviving for 5 days. The differences are due to the larger bottom friction at North Triumph, as discussed later.

The details of the simulations did change with the different settling velocity scenarios. However, the overall character of the simulations remained the same. Overall, the differences between the two settling velocity scenarios had about the same magnitude as the differences due to the different discharge scenarios.

The `bblt` simulations of the barite concentrations during the EEM period were roughly consistent with the EEM observations. Overall the concentrations were small, generally $< 1\ \mu\mathrm{g\,L^{-1}}$. A detailed comparison of the spatial distributions was not done because of the lack of velocity observations leading up to the EEM observations. The results reported here are for our present best estimate of settling velocity. As reported previously (e.g. Gordon et al. (2000); Tedford et al. (2003)) the simulated near-bottom concentrations are very sensitive to settling velocity. Larger settling velocities result in large near-bottom concentration, generally as a result of both reduced dispersion and a reduction in the vertical extent of the concentration profile.

The comparison of the concentrations as a function of distance from the rig was encouraging. Both the observations and the simulations show a general decrease away from the rig with the highest concentrations nearest the rig. A more detailed comparison is confounded by uncertainty over the background values and temporal undersampling in the observations. The observed concentrations were so small that any comparison between the observations and the model needs to account for the natural barium concentration in the suspended particulate matter. Visual inspection of the EEM observations

from June 1999 and October/November 1999 suggests that the appropriate background barium (barite) concentration should be in the range 0.3 - 0.5 $\mu g\,L^{-1}$ (0.5 - 0.8 $\mu g\,L^{-1}$). This is much larger than the 0.25 $\mu g\,L^{-1}$ (0.42 $\mu g\,L^{-1}$) used for barium (barite) in the comparison. However the difference does not affect the conclusions drawn from this study.

As an independent check on the background value, consider the following statistical comparison. The model-based statistics in Figure 15 indicate that during the EEM period the probability of observing barite concentrations in excess of 0.1 $\mu g\,L^{-1}$ above background was about 20% and the probability of observing concentrations more that 1 $\mu g\,L^{-1}$ above background was less than 5%. Given 30-40 EEM samples the model predicts about 7 samples with concentrations 0.1 $\mu g\,L^{-1}$ above background and 1-2 samples 1 $\mu g\,L^{-1}$ above. In terms of barium concentration (recall the conversion factor of 1.7), we expect 3-4 samples 0.1 $\mu g\,L^{-1}$ above background and about 1 sample 1 $\mu g\,L^{-1}$ above. This is broadly consistent with the EEM results in Figure 11 assuming a background barium concentration of 0.4-0.5 $\mu g\,L^{-1}$.

The simulated near-bottom concentrations (bottom 10 cm) were similar to those at 0.5 mab except that they were a little larger. As with the concentrations at 0.5 mab, the near-bottom concentrations were much larger during the early part of the simulation when the discharges were higher. The exposure time maps show concentrations in excess of 100 $\mu g\,L^{-1}$ (the no effects concentration for scallops) extending to the south and southwest of the rig. Overall the exposure times are not very long. Using the 50 hour (2 day) isoline for reference, Figures 19, 20, 21 and 22 indicate that the area with concentrations greater than 100 $\mu g\,L^{-1}$ extends between 1 and 6 km to the south. The region affected for longer times and/or by larger concentrations is less than this.

The timing of the EEM observations relative to the discharges makes it difficult to provide a strong test of the model. The model suggests that the concentrations decrease rapidly during the first two days of the EEM observations. In general the observed concentrations are so small that it is difficult to know how many samples are actually above the background value. In addition, the loss of the ADCP during the simulation period weakens the comparison between the model and the observations. In this case, the ADCP was disabled by a large storm. Further model validation using the EEM data will be plagued by similar data problems. Of all the SOEI EEM data from 1998-99, this data set comes closest to having a coincidence between drilling, ADCP measurements and EEM observations.

Tedford et al. (2002, 2003) used `bblt` to investigate the drift and dispersion of drilling muds at Hibernia. They did not have a discharge time series and so used bulk releases and 5 day simulations to characterized the drift and dispersion. They found the effective diffusivity to be small, typically below 5 $m^2\,s^{-1}$ for the slow settling velocity ($w_1 = 0.01$ cm s^{-1}) and below 2 $m^2\,s^{-1}$ for the fast one ($w_0 = 0.05$ cm s^{-1}). Similar simulations were performed at North Triumph for the combined TS2 and TS3 time period and the

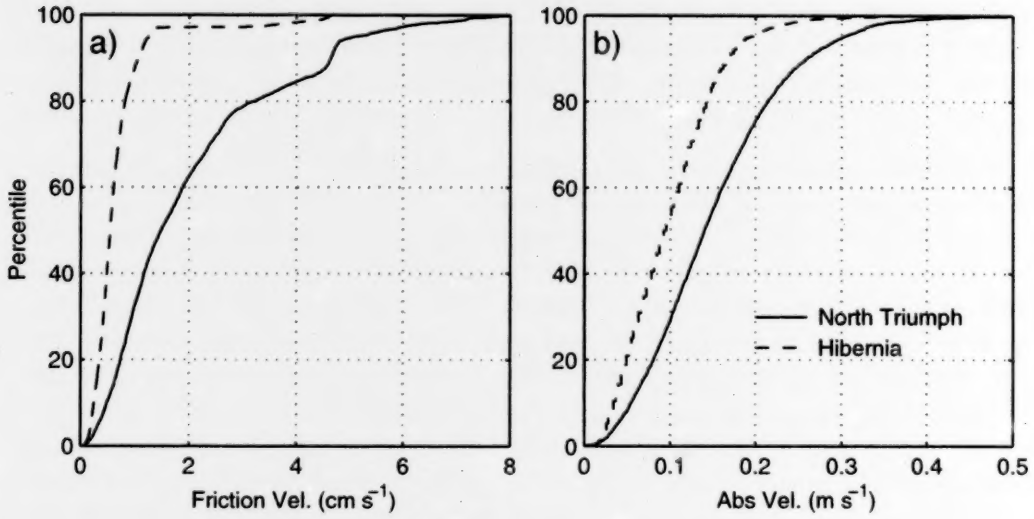

Figure 24: Shown are percentiles for a) the friction velocity and b) 3 mab currents at North Triumph and Hibernia.

corresponding effective diffusivities were 30 and 20 m^2 s^{-1}, roughly an order of magnitude larger.

One difference in the simulations at the two locations is that only 3 and 10 mab current data were available from Hibernia. The currents above 10 mab were estimated using an exponentially decaying shear. To investigate the sensitivity of the effective diffusivity to the currents above 10 mab, velocity time series were created at North Triumph using the 3 and 10 mab currents and the same procedure as used at Hibernia. The results depend on the settling velocity (which controls the vertical extent of the sediment), the imposed maximum height, and the currents (TS2 or TS3). In general, the results change by a factor of order 1 rather than by orders of magnitude. Thus the limited vertical resolution at Hibernia is not likely the primary source of the different effective diffusivities.

The crucial difference is that the currents and bottom stress were generally much larger at North Triumph than Hibernia (Figure 24). There are many more high stress events at North Triumph. In fact, 90% of the u_{*cw} value at Hibernia are < 1 cm s^{-1} whereas at North Triumph the 90th percentile is 4.5 cm s^{-1}. The currents at 3 mab are also much stronger at North Triumph than Hibernia. Thus less wave activity is required to reach the u_{*c}. In addition, if we characterize large wave events as times with a significant wave height greater than 3 (4) meters, then in the fall of 1999 there were large wave events 33% (12%) of the time at North Triumph and 20% (6%) of the time at Hibernia. Thus large wave events appear to be more frequent at North Triumph than at Hibernia. This seems inconsistent with wave climatologies (e.g. Canadian Climate Centre (1991)) which show the wave height for the 50 year event to be about 14 m at

Hibernia and 11 m near Sable Island. While the difference might be due to conditions in 1999, preliminary comparison of the MANMAR data and AES40 hindcast data at Hibernia suggests that the MANMAR significant wave heights are systematically smaller then the AES40 wave heights. Sorting this out is beyond the scope of this report.

The present results for North Triumph are for fall when storm and wave influences on flocculation, suspension and dispersion are expected to be greater than in typical late-spring or summer conditions. For example, the result that the survival time for flocs is of order hours is clearly inconsistent with the observations (Muschenheim and Milligan, 1996) in August 1993 of a thin, dense and persistent layer of flocculated material near the seabed in the area around the Cohasset-Panuke site to the northwest of North Triumph (with water depth approximately 40 m). The friction velocities at Cohasset-Panuke (e.g. Anderson 2001) are generally expected to comparable to those estimated here for North Triumph. The greater degree of flocculation (and larger effective settling velocity) at Cohasset-Panuke during summer 1993 is probably a result of drilling mud discharges during the quiescent summer period (there was limited storm and wave activity that year), which contrasts the fall 1999 period when storms and large waves occurred near the end of the discharge period.

A preliminary analysis of the currents at North Triumph suggests that inertial oscillations and internal tidal currents were a significant component of the currents and the friction velocity. As these processes are intermittent, it is not clear whether the large friction velocities from the fall of 1999 can be generalized to other locations and times of year. The results for North Triumph should be viewed as reflective of fall-winter conditions at that site and others with comparable water depths along the southern side of Sable Island Bank. However, the 1993 Cohasset-Panuke observations suggest that suspension and dispersion are probably substantially reduced during summers (and perhaps other seasons) with reduced storm and wave influences.

An earlier application of the `bblt` model to Georges Bank (Loder et al., 1998; Gordon et al., 2000; Cranford et al., 2003) used constant settling velocities of 0.1 and 0.5 cm s^{-1} to bracket the expected range. At the sites in the mixed areas and in the frontal zone (typically less than 100 m depth), the friction velocities were generally in excess of 1 cm s^{-1} (often 2-4 cm s^{-1}). Based on the stress dependent settling velocity, we would expect the dense drill mud flocs to break up, the barite to act as a single grain, and the effective settling velocity to be closer to 0.1 cm s^{-1} than 0.5 cm s^{-1}. Thus the findings of Gordon et al. (2000) and Cranford et al. (2003), that with a settling velocity of 0.5 cm s^{-1}, scallop populations near a rig in the frontal zone on Georges Bank could experience potential growth inhibition of 10 days during a 93 day drilling scenario is conservative. The friction velocity calculations ignored wave influences on bottom stress and used a simple quadratic drag law with a drag coefficient twice as large as large as the value in SEDTRANS for the currents only case. However, given that these two effects act in opposite directions and the large currents in the frontal zone on Georges Bank, we do not expect that a recalculation would reduce the friction velocities to below the floc breakup

value of 1 cm s^{-1}. At the deeper sites on Georges Bank, the currents are smaller and the details of the stress calculation will affect the magnitude of the friction velocity relative to the floc breakup value. Thus we cannot discount the possibility of the larger settling velocity.

Assembling accurate drilling waste discharge time series has been a major task in this project. The records for the Venture wells (not reported here) often glossed over the volumes of water-based mud (WBM) sent overboard. By the time the North Triumph well NT-1 was drilled, the fluids discharge logging had become more thorough. Nevertheless we were forced to go to records of materials shipped, returned, etc., to assemble estimates of what the true discharge was. Our assessment of the North Triumph records resulted in high (212 tonnes) and low estimates (60 tonnes) of the discharges that differed by 152 tonnes of barite.

5 Conclusions

The primary conclusions of the study are:

1. The `bblt` model predicts that discharged drilling muds drifted and dispersed from the North Triumph well site in fall 1999 on the time scale of days to weeks. The simulations indicate that near-bottom (lower 10 cm) barite concentrations at particular locations only exceeded the laboratory threshold value for impairment of scallop growth (100 $\mu g\, L^{-1}$) for total times of the order of days at positions within several kilometers of the well site.

2. The simulated barite concentrations at 0.5 mab are generally consistent with the concentrations observed during the EEM survey in late October and early November 1999. In particular, there is consistency in the prediction and observation of very low concentrations, substantial spatial and temporal variability, and a general tendency for concentrations to decrease with distance from the well site. These results provide further support for the utility of the `bblt` model in environmental assessment and monitoring programs, although there remain limitations and uncertainties.

3. The model evaluation has been limited by the various observational datasets available for forcing the model and describing the spatio-temporal evolution of the discharged muds. There were difficulties in obtaining critical data on the discharge rates and timings, such that two discharge scenarios differing in total volume by a factor of 3-4 had to be used. There was misfortune in the loss of the moored ADCP and wave buoy during a storm near the end of the primary discharge period. The missing currents data was particularly problematic and a stochastic approach had to be used in the model evaluation involving an ensemble of synthetic currents times

series. Considering the model prediction of strong variability in mud suspension and concentrations, there was severe undersampling of suspended mud concentrations in the EEM survey such that spatial and temporal variability are probably highly convoluted in those observations.

4. Because the EEM survey was not carried out until about 3 weeks after the peak discharges, there are no observations to evaluate the model predictions of barite concentrations greater than 100 $\mu g\,L^{-1}$ (the effects threshold for scallop growth impairment) for a few days within several kilometers of the well site.

5. Careful logging of discharges, and concurrent Physical Environmental (currents, waves) and EEM observations from the beginning of the discharge period to several weeks beyond the end of significant drilling discharges, combined with the application of drift and dispersion models, such as `bblt`, provides the potential to reduce the uncertainties in the predictive capability of the fate and effects of drilling mud discharges.

6. The AES 40 hindcast predictions of waves near the North Triumph site in fall 1999 are in good agreement with buoy observations from the Physical Environmental program. This supports their use in `bblt` applications at other times and locations.

7. The results presented here for the fall of 1999, should be viewed as reflective of fall-winter conditions at North Triumph and other sites with comparable water depths and stratification along the southern side of Sable Island Bank. The inertial oscillations and internal tidal currents identified in the preliminary analysis as a significant factor in the observed currents are intermittent processes. It is not clear whether the large friction velocities that contribute to the short life time of the fast settling flocs can be generalized to other locations and times of the year.

8. Comparisons with previous `bblt` simulations at Hibernia indicate that dispersion at the North Triumph site (at least during fall 1999) was significantly higher than at Hibernia in a similar water depth on the northeast Grand Bank (Tedford et al., 2002, 2003). This was primarily due to stronger currents (particularly tidal) on Sable Island Bank, but there is also a suggestion of larger waves at North Triumph in fall 1999. The latter is opposite to expectations based on wave climatologies and is being investigated.

9. Initial comparisons with previous `bblt` applications to Georges Bank (Gordon et al., 2000; Cranford et al., 2003) indicate that the range of temporal variability in near-bottom horizontal dispersion rates at North Triumph in fall 1999 is comparable to the range of dispersion rates across the Northeast Peak of Georges Bank. Further, the recent findings (e.g. Hill et al. (2001)) that suspended sediment flocs are rapidly broken up when the friction velocity exceeds 1 cm s^{-1} indicates that the cases with a settling velocity of 0.1 cm s^{-1} are likely to be more realistic than those with 0.5

cm s^{-1}. This suggests that the Gordon et al. (2000) and Cranford et al. (2003) conclusions regarding potential impacts on scallops in the frontal zone on Georges Bank were likely conservative.

Acknowledgments We are grateful to the Environmental Sciences Research Fund (ESRF) for funding this evaluation study, and to the Offshore Environmental Impacts POL (Program at Objective Level) of the federal Program on Energy Research and Development (PERD) for supporting the development, recent improvement and ongoing evaluations of the bblt model. We are also grateful to colleagues at Sable Offshore Energy Incorporated (SOEI), Coastal Oceans Associates (COA), Jacques Whitford Environmental Limited (JWEL), and MI-SWACO for cooperation and assistance with the project. We particularly thank Cal Ross (SOEI), Geoff Hurley (formerly with SOEI), Patrick Roussel (COA), and Blake Brockerville (MI-SWACO) in this regard. We thank Phil Yeats (BIO) for suggesting the use of the aluminium/barium relationship as a way to detect elevated levels of barium in the sediment and Tim Milligan (BIO) for ongoing discussions. We also thank former colleagues Sean Oakey (Harding Technical and Scientific Services) and Ted Tedford (Evans Consulting Ltd.) for input to early phases of the study.

References

Anderson, C. 2001. Seabed shear stress estimates at the Cohasset and Hibernia oil production sites. Can. Data Rep. Hydrogr. Ocean Sci. 216:viii+54pp.

Canadian Climate Centre. 1991. Wind/wave hindcast extremes for the east coast of Canada, Volume I. Prepared under contract no. KM169-7-6678 by MacLaren Plansearch Ltd. and Oceanweather, Inc., 109 p. plus appendices.

Coastal Ocean Associates Inc. (COA). 2000. Physical Oceanographic Data Report: 1999 Current Data - North Triumph. 13 pp + Appendices. Report Prepared for Seimac Ltd., Dartmouth N.S. on behalf of Sable Offshore Energy Inc., Halifax N.S.

Cranford, P.J., Gordon, D.C. Jr., Lee, K., Armsworthy, S.L., and Tremblay, G.-H., 1999. Chronic toxicity and physical disturbance effects of water- and oil-based drilling fluids and some major constituents on adult sea scallops (*Placopecten magellanicus*). Mar. Env. Res., **48**: 225-256.

Cranford, P.J., D.C. Gordon Jr., C.G. Hannah, J.W. Loder, T.G. Milligan, D.K. Muschenheim, and Y. Shen. 2003. Modelling Potential Effects of Petroleum Exploration Drilling on Northeastern Georges Bank Scallop Stocks. Ecological Modelling. In press.

Gordon Jr., D.C., Cranford, P.J., Hannah, C.G., Loder, J.W., Milligan, T.G., Muschenheim, D.K., and Shen, Y. , 2000. Modelling the transport and effects on scallops of water-based drilling mud from potential hydrocarbon exploration on Georges Bank. Can. Tech. Rept. Fish. Aquat. Sci., 2317: 115 pp.

Hannah, C.G., Y. Shen, J.W. Loder and D.K. Muschenheim. 1995. `bblt`: Formulation and Exploratory Applications of a Benthic Boundary Layer Transport Model. Can. Tech. Rep. Hydrogr. Ocean Sci. 166: vi + 52 pp.

Hill, P. S., J. P. Syvitski, E. A. Cowan and R. D. Powell. 1998. In situ observations of floc settling velocities in Glacier Bay, Alaska. *Marine Geology*, **145**: 85-94.

Hill, P. S., T. G. Milligan, and W. R. Geyer. 2000. Controls on effective settling velocity of suspended sediment in the Eel River flood plume. *Cont. Shelf Res.*, **20**: 2095-2111.

Hill, P. S., G. Voulgaris, and J. H. Trowbridge. 2001. Controls on floc size in a continental shelf bottom boundary layer. *J. Geophys. Res.*, **106**: 9543-9549.

Li, M.Z. and C. L. Amos. 2001. SEDTRANS96: the upgraded and better calibrated sediment-transport model for continental shelves. *Comput. Geosci.*, **27**: 619-645.

Loder, J.W., C. G. Hannah, Y. Shen, E. A. Gonzalez, Z. Xu. 1998. Suspended sediment drift and dispersion on Georges Bank. Unpublished manuscript with 188 pages. Many of the results were reported in Gordon et al. (2000).

MacLaren Plansearch, 1997. Phase B - Impact assesment final report, Physical fate of drilling and production effluent discharges and impact on marine environment, Part 1: Drilling waste discharges.

Milligan, T. G. and P. S. Hill. 1998. A laboratory assessment of the relative importance of turbulence, particle composition, and concentration in limiting maximal floc size and settling behaviour. *J. Sea Research* **39**: 227-241.

Milligan, T.G., D. Belliveau, D.K. Muschenheim and G.R. Morton. 1998. New equipment for benthic habitat studies. *Sea Technology*, **39**: 56-61.

Muschenheim, D.K. and Milligan, T.G., 1996. Flocculation and accumulation of fine drilling waste particulates on the Scotian Shelf (Canada). Mar. Pollut. Bull., **32**:740-745.

Rouse, H. 1937. Modern concepts of the mechanics of turbulence. *Trans. Am. Soc. Civ. Eng.*, **102**, 463–543.

Sable Offshore Energy Incorporated. Offshore Environmental Effects Monitoring Program (1999 Annual Report): Venture, Thebaud & North Triumph. March 2000. Report prepared by Jacques Whitford Environment Limited, Dartmouth N.S.

Swail, V.R., V.J. Cardone and A.T. Cox. 1998. A Long Term North Atlantic Wave Hindcast. Fifth International Workshop on Wave Hindcasting and Forecasting. January 26-30, 1998. Melbourne, Florida.

Swail, V.R. and A.T. Cox. 2000. On the use of NCEP/NCAR Reanalysis Surface Marine Wind Fields for a Long Term North Atlantic Wave Hindcast. J. Atmo. Tech. **17**, 532–545.

Tedford, T., E. Gonzalez, and C. G. Hannah. 2001. `bblt` Version 3.1 User's Manual. Can. Tech. Rep. Hydrogr. Ocean Sci. 213: v + 48 pp.

Tedford, T., C. G. Hannah, T. G. Milligan, J. W. Loder, and D.K. Muschenheim. 2002. Flocculation and the fate of drill mud discharges. In: Estuarine and Coastal Modelling: Proceedings of the 7th International Conference (St. Petersburg Fl., 5-7 November, 2001). M.L. Spaulding (Editor). ASCE. 294-309 pp.

Tedford, T., A. Drozdowski and C. G. Hannah. 2003. Suspended sediment drift and dispersion at Hibernia. Can. Tech. Rep. Hydrogr. Ocean Sci. 227: vi + 57 pp.

Thomson, D.H., R.A. Davis, R. Belore, E. Gonzalez, J. Christian, V.D. Moulton, and R.E. Harris. 2000. Environmental Assessment of Exploration Drilling Off Nova Scotia. Report prepared for Canada - Nova Scotia Offshore Petroleum Board and Mobil Oil Canada Properties, Shell Canada Ltd., Imperial Oil Resources Ltd., Gulf Canada Resources Ltd., Chevron Canada Resources, EnCana Petroleum Ltd., Murphy Oil Company Ltd., and Norsk Hydro Canada Oil & Gas Inc. Reported prepared by LGL Ltd. Environmental Research Associates, LGL Report, TA 2281: x+280 p.

A Details of Gap Filling and Vertical Extrapolation of the ADCP Data

TS2 was found to have data gaps at all depths below 21 mab (Table 5). These gaps were interpolated in order to meet the requirement for temporal uniformity in `bblt`. The interpolation method is described in this appendix.

An additional difficulty with TS2 was the absence of currents below 8 mab. `bblt` assumes a log layer below the lowest level of specified currents and it was not clear that the 8 mab current would be in the log layer. This appendix also describes how the TS3 data, which has currents between 8 mab and 3 mab, were used to estimate TS2 currents between 3 and 7 mab.

Gap Filling

The gap filling down to 8 mab was done by using linear regression to relate the currents at 21 mab with those at each of the levels below. The regression was done using the complex velocity $u + iv$ so that the rotations of the velocity vector were handled in a natural manner.

Let ϕ be the (complex) velocity at 21 mab and w be the velocity at the level requiring gap filling. The procedure for gap filling as follows

1. Perform a tidal analysis and remove the tidal currents (ϕ_t and w_t) from each time series to obtain the residuals:

$$\phi_r = \phi - \phi_t \tag{3}$$
$$w_r = w - w_t \tag{4}$$

2. Use the gap free sections of w_r, the corresponding sections of ϕ_r, and linear regression, to compute the complex coefficients m and c, that minimizes the velocity error $w'_r - w_r$ in the least square sense. The estimated time series at the required level is then

$$w'_r = m\phi_r + c \tag{5}$$

3. Use (5) to generate the missing section of w_r.

4. Finally add back the tidal contribution:

$$w' = w'_r + w_t \tag{6}$$

with w_t taken from step 1.

Table 5: Classification of gaps in TS2

MAB	GAP#	START	END
8	1	274.208	274.583
8	2	276.708	277.083
8	3	282.042	282.417
8	4	287.500	288.042
8	5	290.417	292.292
Percent of Total:			16.4
9	1	276.500	277.125
9	2	287.500	288.083
9	3	290.458	292.292
Percent of Total:			14.1
10	1	276.708	277.083
10	2	287.500	288.042
10	3	290.500	292.292
Percent of Total:			12.6
11	1	276.708	277.083
11	2	287.500	287.917
11	3	290.458	291.542
11	4	291.542	292.292
Percent of Total:			12.0
12	1	276.708	277.125
12	2	287.500	287.917
12	3	290.500	291.542
12	4	291.583	292.292
Percent of Total:			12.0
13	1	287.500	287.875
13	2	290.750	291.542
13	3	291.625	292.292
Percent of Total:			8.5
14	1	287.500	287.875
14	2	290.750	291.542
14	3	291.708	292.292
Percent of Total:			8.1
15	1	287.500	287.875
15	2	290.875	291.542
15	3	291.667	292.292
Percent of Total:			8.3
16	1	290.917	291.542
16	2	291.708	292.292
Percent of Total:			5.6
17	1	290.917	291.542
17	2	291.708	292.292
Percent of Total:			5.6
18	1	290.917	291.500
18	2	291.750	292.292
Percent of Total:			5.2
19	1	290.958	291.500
19	2	291.750	292.167
Percent of Total:			4.3
20	1	290.917	291.333
20	2	291.750	292.167
Percent of Total:			3.9

The time series of speed at selected levels are shown in Figure 25. The data in the gaps is shown in red. The regression coefficients and a measure of the error are listed in Table 6.

The procedure used the lowest level with continuous data returns (21 mab) to predict the currents at all the depths below. An alternative procedure would have been to work in an iterative fashion; use the data at 21 mab to fill the gaps at 20 mab, and then use the data at 20 mab to fill the gaps at 19 mab and so on. This was not pursued.

Vertical Extrapolation

Figure 26 shows that for TS3 the currents below 8 mab are highly correlated with the currents at 8 mab. Visually the correlation is strong at 7 mab and degrades with distance. The missing levels of TS2 (3, 4, 5, 6 and 7 mab) were filled as follows. Use TS3 to build a statistical model of the relationship between the currents at 8 mab and those at the other levels. Then use these relationships to project the 8 mab currents to the other levels for the TS2 period.

The statistical model was built using the complex velocity $w = u + iv$ where u and v are the eastward and northward and velocity components and $i = \sqrt{-1}$. The complex velocity was used so that the statistical model would naturally allow for rotations in the velocity vector as well as amplitude changes.

Let ϕ_3 be the observed (complex) currents at 8 mab for TS3 and w_3 be the TS3 currents at one of the unknown levels of TS2. The basic data model is

$$w_3' = m\phi_3 + c \tag{7}$$

where w_3' is the best fit of the current at the specified level to the linear model based on the 8 mab currents and m and c are the (complex) coefficient for that level found by minimizing the total velocity error $w_3' - w_3$ in the least square sense.

Let ϕ_2 be the TS2 currents at 8 mab. The unknown TS2 currents below 8 mab (w_2') are estimated from

$$w_2' = m\phi_2 + c. \tag{8}$$

where m and c are the coefficients for the appropriate level.

The coefficients and the relative errors are listed in Table 6 (7 mab and below). The errors were computed by comparing the estimated TS3 velocity from (7) with the observed TS3 velocity. This is clearly an underestimate of the minimum error as the gap filling of the TS2 currents at 8 mab introduces errors, and the relationships between the 8 mab currents and those below could have changed between TS2 and TS3.

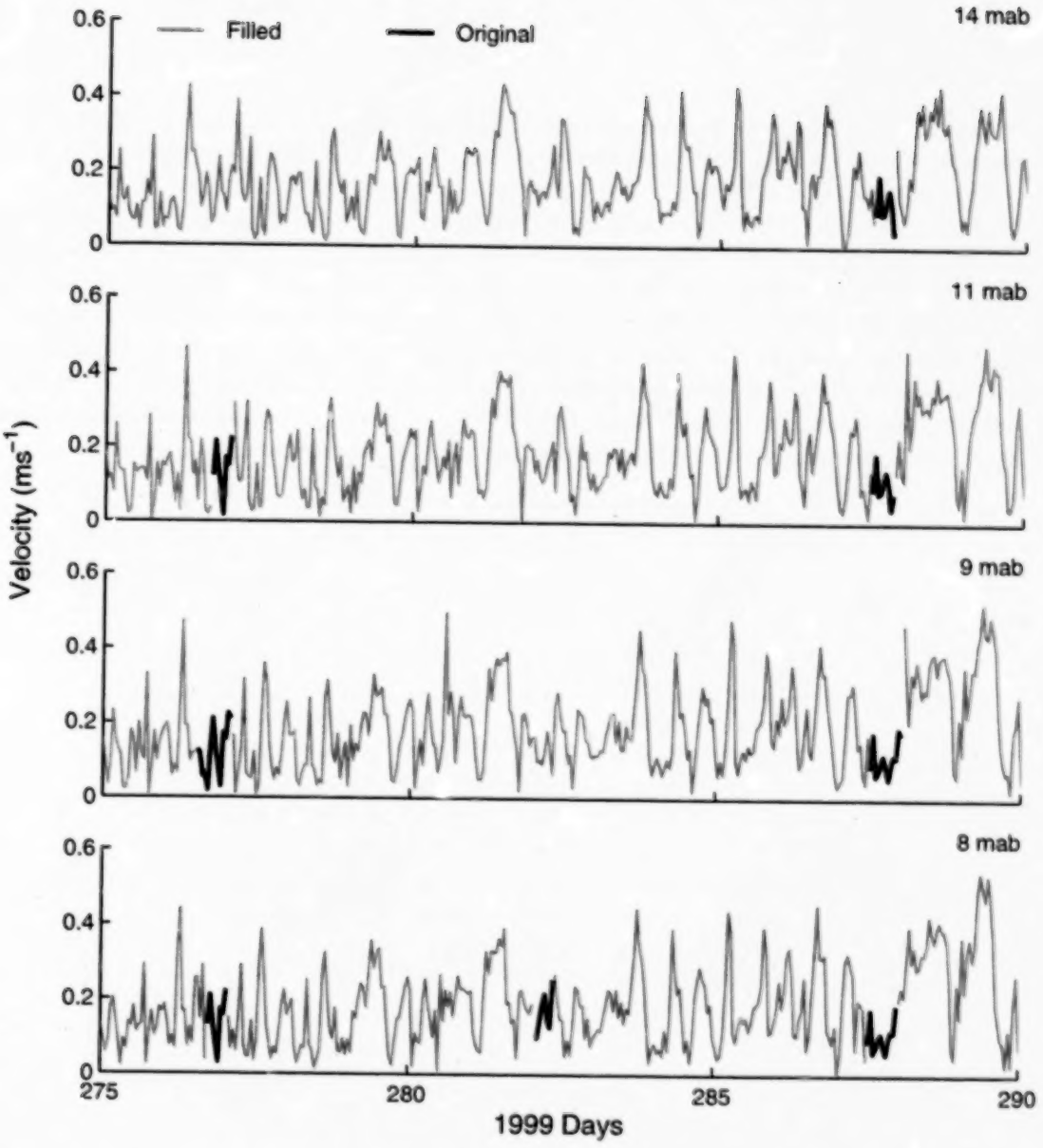

Figure 25: The residual current (w_r and w'_r) speed at selected depths for TS2. The observations are the grey lines and the estimated currents in the gaps are in black.

Table 6: Least square fit parameters and relative rms errors for $w'_r - w_r$ for the gap filling and $w' - w$ for vertical extrapolation procedure. The real and imaginary parts of the parameters m and c are shown. The error was defined as $(RMS(w'_r - w_r)/RMS(w_r))$ for gap filling and as $(RMS(w' - w)/RMS(w))$ for the vertical extrapolation. The gap filling error (8 mab and above) was computed with the formula $(RMS(w'_r - w_r)/RMS(w_r))$ by comparing the estimated currents with the known currents where they exist in TS2. The error for the missing levels below 8 mab is calculated with the formula $RMS(w' - w)/RMS(w)$ from the TS3 data. It's clearly an underestimate of the error as 1) portions of the 8 mab TS2 level were filled with 21 mab TS2 level and 2) we used TS3 to make conclusions about the vertical structure of TS2. The table is divided between 3-7 and 8-21 mab to emphasize the different methods and error metrics.

mab	Re(m)	Im(m)	Re(c)	Im(c)	Error
20	0.998	-0.009	0.006	-0.003	0.126
19	1.000	-0.005	0.010	-0.003	0.184
18	1.006	-0.009	0.013	-0.005	0.230
17	0.986	-0.004	0.017	-0.006	0.313
16	0.985	0.003	0.021	-0.007	0.353
15	0.984	0.021	0.024	-0.006	0.409
14	0.961	0.025	0.027	-0.005	0.453
13	0.948	0.032	0.032	-0.008	0.493
12	0.924	0.051	0.033	-0.006	0.541
11	0.898	0.064	0.033	-0.008	0.575
10	0.884	0.063	0.041	-0.005	0.622
9	0.866	0.062	0.049	-0.006	0.647
8	0.835	0.080	0.052	-0.009	0.660
7	0.980	0.010	0.006	-0.001	0.169
6	0.948	0.025	0.012	-0.000	0.266
5	0.895	0.042	0.017	0.000	0.353
4	0.828	0.052	0.022	0.002	0.429
3	0.741	0.059	0.025	0.005	0.500

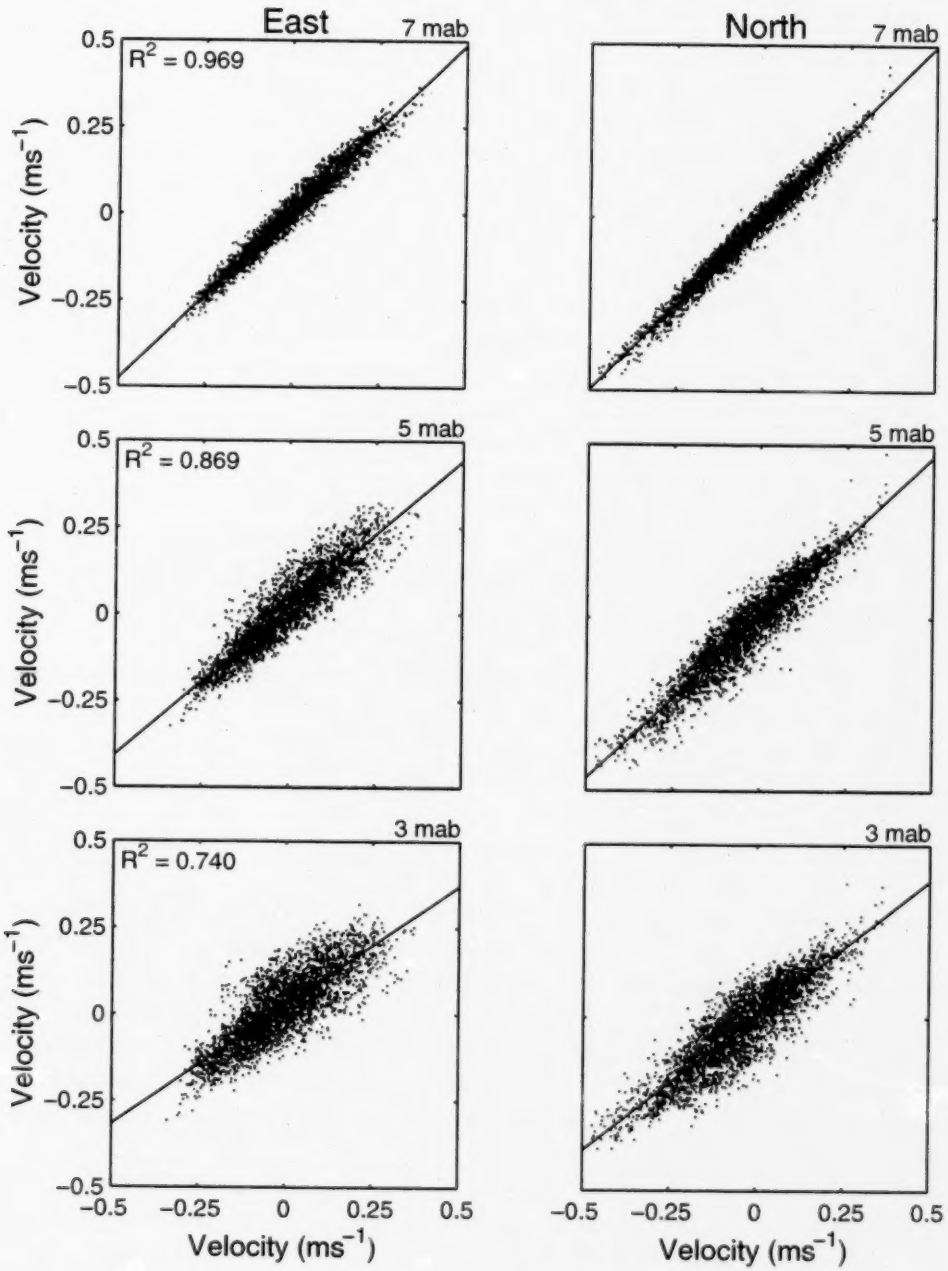

Figure 26: East and North TS3 current below 8 mab (7,5 and 3) plotted versus the 8 mab current. The solid lines show the least squares fits with the two velocity components plotted separately. R^2 is the fraction of the variance explained by the linear fit.

B Details of Extrapolation in Time of the ADCP Data

No currents data were available for the period from October 19 to November 18, 1999 prompting us to develop a method for generating synthetic current time series using the observations before and after the gap (TS2 and TS3). The following steps were taken to generate the synthetic time series:

1. A tidal analysis of the TS2 currents at 3 mab was performed and the tidal residual computed: $w_r = w - w_t$. The velocity is again written in complex form $(u + iv)$ and the notation is similar to that used in the previous section.

2. The complex frequency spectrum (amplitude and phase) of w_r was computed using an FFT.

3. The phase at each frequency was replaced by a randomly generated phase between $-\pi$ and π. Analysis showed that there was very little correlation between neighbouring phases.

4. The differences between the new phases and the original phases were saved.

5. A new time series w_r' was constructed for the period October 19 to November 10 using the inverse FFT. This doubled the length of TS2.

6. Tidal prediction was used to generate the tides for the same period.

7. The tidal prediction was combined with the new residual to produce a synthetic current time series for the period October 19 to November 10. This new time series represents the forward time extrapolation of the TS2 currents at 3 mab.

8. Levels above 3 mab were filled in the same manner but instead of using random phases, the phase differences computed in step 4) were subtracted from the FFT phase. This preserves the vertical structure of the phase and avoids introducing additional vertical shear.

9. The above steps were repeated for TS3 to generate the backward extrapolation extending from November 18 back to October 19 (doubling the length of TS3).

10. The forward (TS2) and backward (TS3) extrapolations were combined in such a way that TS2 filled the left half of the gap and TS3 the right. To avoid a discontinuity in the center, the two were combined gradually in a 20 hour window using linear interpolation.

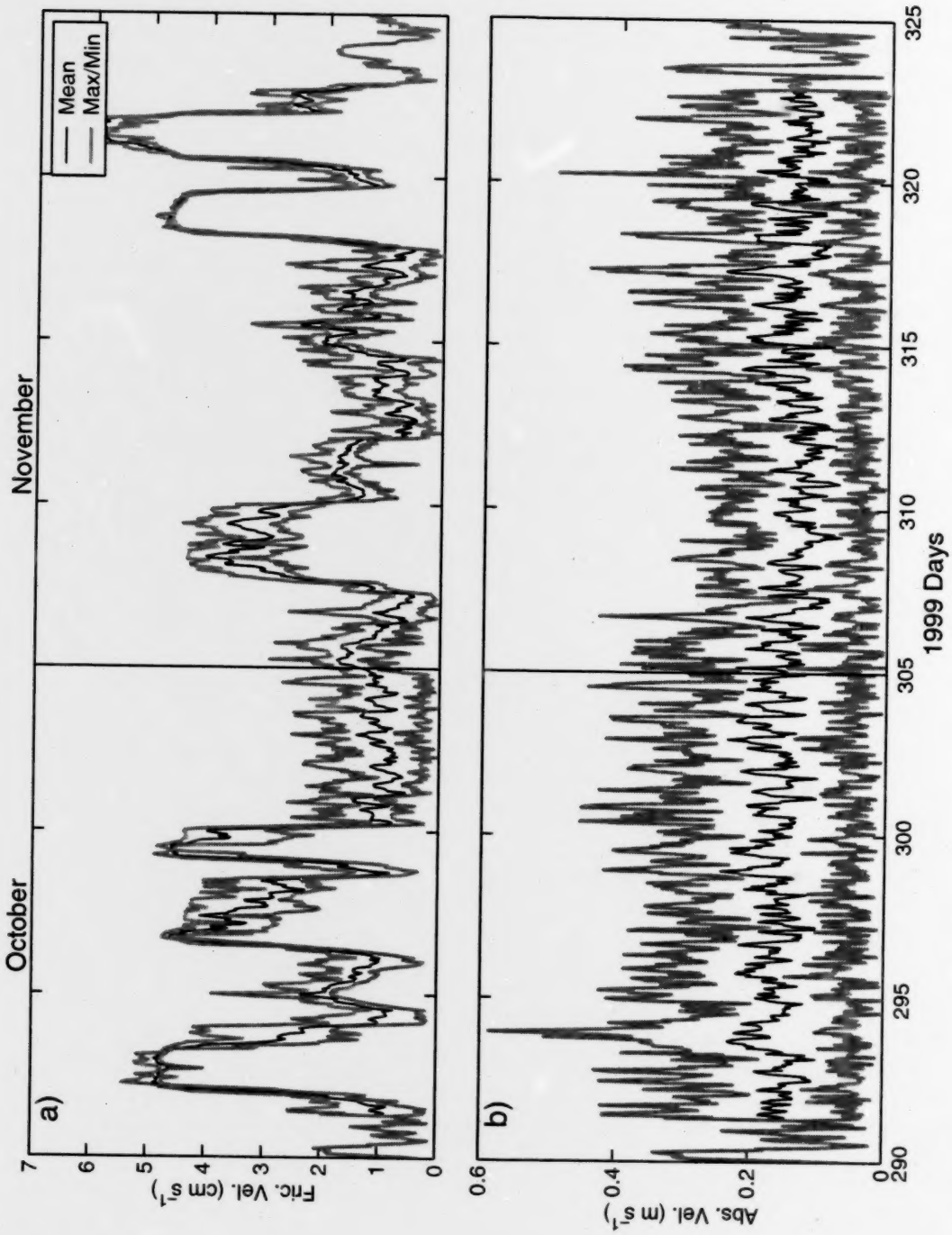

Figure 27: Statistics of a) friction velocity (u_{*cw}), based on 10 realizations of the synthetic currents and b) speed at 3 mab.

Ten realizations of the synthetic currents in the gap were generated through repeat of steps 3-10 with different randomly generated phases. Figure 27 shows the mean, maximum and minimum values of the 3 mab currents. Also shown are the resulting statistics for the bottom stress (u_{*cw}).

C Vertical Profiles at North Triumph

Here we show a vertical profiles of the currents for selected periods (Figure 28). The mean profiles averaged over the TS2 and TS3 periods have similar vertical structure with flow to the south in the surface layer, to the west and southwest at mid-depth, and to the southeast at the bottom. The near-bottom layer is thinner in the later period and the mid-depth layer is thicker. The final panel, Figure 28d, represents the currents during the EEM period and is averaged over the 10 synthetic current time series. It is rotated 180° relative to the others reflecting the northward near-bottom flow that occurred in the synthetic currents during the EEM period (Section 3.4).

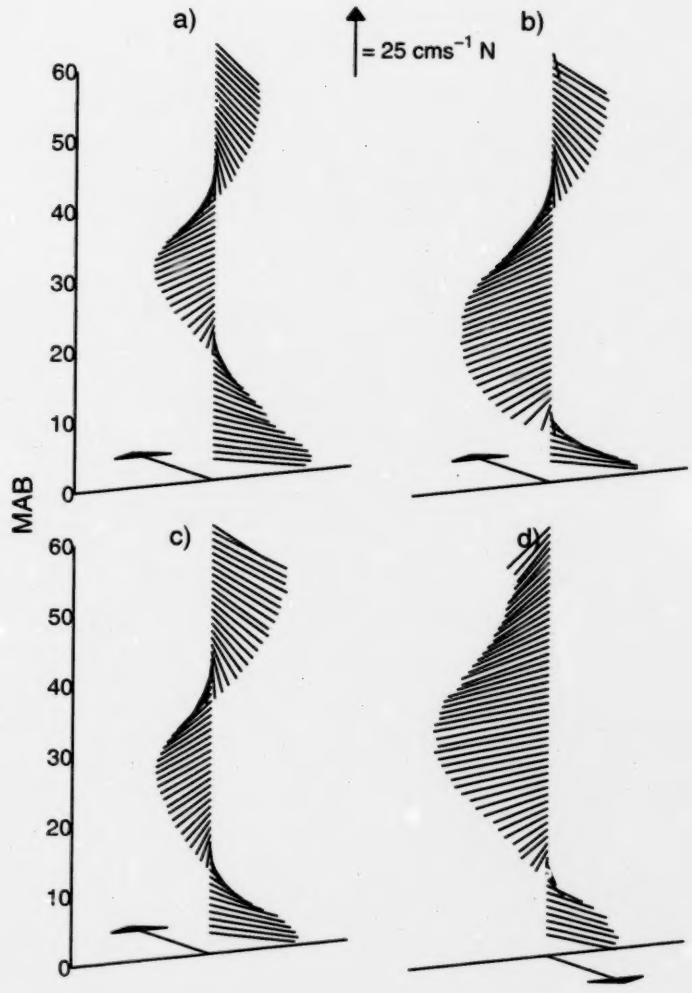

Figure 28: Vertical profiles of mean velocity for a) TS2, b) TS3, c) combined TS2 and TS3 with time extrapolation, and d) 28 Oct. to 5 Nov. 1999. The horizontal arrow indicates 25 cm s^{-1} to the North. The direction of panel d) is rotated relative to the others for display purposes.